CCIT Report #480 April 2004

Spectral Efficiency of Joint Multiple Cell-Site Processors for Randomly Spread DS-CDMA Systems*

Oren Somekh Benjamin M. Zaidel Shlomo Shamai (Shitz)

May 8, 2004

Abstract

We consider a chip-interleaved randomly spread DS-CDMA scheme employed in three variants of Wyner's infinite linear cell-array model with flat fading. Focusing on the asymptotic setup in which both the number of users per cell and the processing gain go to infinity while their ratio (the "cell load") goes to some finite constant, the spectral efficiencies of the optimum and linear MMSE *joint multi-cell receivers* are considered. Dramatic performance enhancement as compared to *single*-cell-site processing is demonstrated. The asymptotic behavior of the two receivers in extreme SNR regimes and in a high cell-load setup are analyzed as well. The impact of chip-interleaving vs. symbol-interleaving is also investigated. Chip-level interleaving is found beneficial in several cases of interests, and is conjectured to be beneficial in general.

*The authors are with the department of Electrical Engineering, Technion - IIT, Haifa 32000, Israel. E-mails: orens@tx.technion.ac.il, bennyz@inter.net.il, sshlomo@ee.technion.ac.il

1 Introduction

One of the most dramatic developments of the past two decades in communications technology is the huge evolvement of cellular communications systems. Cellular systems now offer ubiquitous wireless access to a wide variety of multimedia services, for both outdoor and indoor applications, with a constantly increasing penetration and a growing demand for higher and higher user data-rates. This evolution has led to an abundance of scientific researches in the quest for an efficient utilization of the available bandwidth, thus increasing the capacity of the systems in concern. In particular, within the framework of information theoretic research, the fundamental limits of cellular communications have been explored. One of the major issues to be addressed in cellular systems is the presence of inter-user interference. The nature of inter-user interference depends on the manner in which the available time, frequency and space resources are utilized, and on the feasibility of inter-user/inter-cell-site cooperation. For example, in the cellular uplink channel interference may be generated by other intra-cell users when a Code Division Multiple Access (CDMA) scheme is employed, and by other-cell users when both Frequency/Time Division Multiple Access (F/TDMA) and CDMA schemes are employed (depending obviously on the inter-cell frequency reuse scheme). Similarly, in the cellular downlink channel, unless a coordinated transmission scheme is employed, the user may suffer interference from transmissions of other-cell sites within its neighborhood. Conventionally, as is the case with 2G cellular systems, other-user and other-cell-site interference are treated simply as an additive white Gaussian noise (AWGN), and no receiver/tranmiter cooperation is employed. However, this approach makes the system interference limited, and it is quite clear that in order to meet the growing demand for higher data rates more advanced reception and transmission approaches are called for, that take into account the structure of the channel and the transmitted signals, and employ cooperative processing techniques whenever realizable.

Since the introduction of the IS-95 direct-sequence (DS) CDMA cellular standard in the early 1990's, and its evolution into the 3G cellular standards, there is a growing interest in information theoretic aspects of DS-CDMA systems. The aim is at the fundamental characteristics and limitations of various multiuser detection strategies [1], providing considerable enhancement of system performance as compared to the "conventional" approach.

Focusing on the more practically appealing systems that employ *random* signatures, results of particular interest concern asymptotic conditions at which both the number user per cell and the length of the signature sequences (processing gain) go to infinity, while their ratio (referred to as the *"cell load"*) is kept arbitrarily fixed. These asymptotic conditions enable the harnessing of results from the theory of random matrices, allowing for *analytical* treatment of various system performance indicators. The key here is the property of random matrices of certain structure according to which their empirical eigenvalue distribution, which depends on specific realizations for finite matrices, goes to a limit given by a deterministic probability distribution function, depending only on the statistical properties of the matrices involved (e.g., see [2], [3], [4]). Thus, performance measures which are otherwise dependent on specific signature realizations, can be expressed in terms of deterministic functions which at least in some cases of interest take a closed explicit form.

Seminal results in this framework were obtained by Verdú and Shamai in [5] and [6]. The fundamental figure of merit for system performance is identified as the (per-cell) *spectral efficiency*, defined as the maximum number of bits/sec/Hz (or equivalently bits/chip) that can be transmitted arbitrarily reliably within a cell. In [5], Verdú and Shamai analyze the *uplink* of a single-cell synchronous DS-CDMA system with random spreading sequences, while assuming non-fading channels. Considering the case of equal received powers, which implies a perfect uplink power control, four multiuser detection strategies are analyzed and compared in terms of their resulting spectral efficiency. The authors examine the optimum receiver, the matched filter receiver, the decorrelating detector, and the linear minimum mean squared error (MMSE) receiver. In addition to explicit *analytical* expressions for the spectral efficiencies of the four detection strategies, an asymptotic analysis for cases in which the cell load or $\frac{E_b}{N_0}$ go to infinity is provided, and also a comparison to the spectral efficiency obtained without (the constraint of) random spreading. The results obtained in [5] extend also to the case of *homogeneous fading* where each of the spreading chips is assumed to be affected by i.i.d. fading coefficients with unit variance. In [6], Shamai and Verdú extend their results of [5] to frequency-flat fading channels, while assuming full channel state information at the receiver. Again, the matched filter, the decorrelator, the linear MMSE receiver, and the optimum receiver are analyzed, and spectral efficiency results expressed as a function of the fading distribution are presented. Furthermore, the spectral efficiency slopes of the receivers in extreme SNR regimes are derived, providing

for a deeper understanding of characteristics of the four multiuser detection approaches. Assuming equal average received power, it is shown for the linear MMSE receiver hat fading *increases* spectral efficiency for a high cell load. In contrast, it shown that the optimum receiver cannot benefit from the presence of fading. In addition to the above, the authors analyze the effect of power control (assuming full channel state information at the *transmitter*), and present expressions for the optimum power control functions in terms of spectral efficiency (given as a function of the fading parameters and their statistics). For the optimum receiver, a remarkable result is obtained according to which, at least for Rayleigh fading, the resulting spectral efficiency with optimum power control and a large system load is *higher* than that of the single-user AWGN channel. This result demonstrates the phenomenon of *multiuser diversity*, i.e., splitting power among many users subject to independent fading is beneficial. Another important result of [6] is an explicit relation between the spectral efficiency of the linear MMSE receiver and that of the optimum receiver, considerably simplifying the (numerical) evaluation of the optimum spectral efficiency, and characterizing the loss in spectral efficiency due to the suboptimality of the linear receiver (see also [7] in this respect).

Results related to the ones obtained in [6] are presented in [8]. *Linear* multiuser detection strategies are considered (the linear MMSE receiver, the matched filter receiver and the decorrelating receiver), and the limiting signal-to-interference-plus-noise ratio (SINR) is obtained. Extension of the results of [8] to linear multiuser detectors in a *symbol-asynchronous* but *chip-synchronous* CDMA system is provided by Kiran and Tse in [9]. Extensions to macro- and microdiversity setups, where a multiplicity of receiving antennas is employed, can be found in [10].

Until recently, information theoretic analyses of multiuser detection strategies focused mainly on *single-cell* CDMA systems, in the sense that all users are equivalently treated by the receiver. That is, there is no partition of the users to intra-cell vs. other-cell users, with respect to which different knowledge at the receiver regarding the structure of transmissions may be assumed. The main difficulty in multi-cell analyses, that take into consideration inter-cell interference, is in the definition of an appropriate system model, that gives insight into practical "real life" systems on one hand, but on the other hand still allows for analytical tractability (at least in part) without resorting to tedious numerical simulations. An attractive model for a multi-cell system, which addresses the above "guidelines", has

been presented by Wyner in [11]. In his paper, Wyner proposes a model according to which the system's cells are ordered in either a linear (one-dimensional) cellular array, or in the familiar two-dimensional hexagonal cellular pattern (both patterns are assumed to be infinite). It is assumed that only adjacent cell interference is present and characterized by a single parameter, a scaling factor α, lying between zero and unity. Accordingly, assuming non-fading channels, the received signal at some arbitrary cell-site is given by the signals received from intra-cell users, plus the signals of the interfering users of adjacent cells, as received at their cell sites, multiplied by the above scaling factor. As can be seen there is a total of two interfering cells in the linear array model, and six interfering cells in the hexagonal model. Considering a "wideband" CDMA-like transmission, where all bandwidth is available for coding (as opposed to random spreading), the throughput obtained with optimum *joint* processing of the received signals from *all* cell-sites is derived. The results are compared to those obtained with simpler schemes such as intra-cell TDMA, and with a simpler receiver that passes the signals received at all cell sites through an MMSE based filter. These results are extended to flat-fading channels (assuming again no spreading is employed) in [12] and [13].

In [13] Shannon-theoretic limits on the achievable throughput for Wyner's linear and hexagonal model in the presence of fading are presented. In this framework, the intra-cell TDMA and the wideband protocols are considered, where the maximum reliably transmitted equal rate achieved with joint multiple-cell-site processing (which is also aware of the channel realizations) is used as a figure of merit. Bounds to this rate are found for the intra-cell TDMA protocol by incorporating information-theoretic inequalities and the *Tchebycheff-Markov* moment theory as applied to the limiting distribution of the eigenvalues of a quadratic form of tri-diagonal random matrices. The results are demonstrated for the special case where the amplitudes of the fading coefficients are drawn from a *Rayleigh* distribution, i.e., *Rayleigh* fading. For this special case, it is observed the fading may increase the maximum equal rate, for a certain range of α as compared to the non-faded case. In this setting, the wideband strategy, which achieves the maximum reliable equal rate of the model, is proved to be superior to the TDMA scheme. An upper bound to the maximum equal rate of the wideband scheme is also obtained. This bound is asymptotically tight when the number of users is large ($K \gg 1$). The asymptotic bound shows that the maximum equal rate of the wideband scheme in the presence of fading is higher

than the rate which corresponds to the non-faded case for any inter-cell interference factor $\alpha \in [0, 1]$ and SNR values. This result is found to be independent of the statistics of the fading coefficients.

Although the analyses of [11] – [13] are devoted to wideband transmission schemes, the Wyner multi-cell model can be readily applied to DS-CDMA systems employing random spreading sequences. In this framework, the results of [5] and [6] were extended to Wyner's linear cell-array model in [14] and [15], for non-fading and flat-fading channels, respectively. Confining the discussion to *single cell-site processing*, four multiuser detection strategies are considered: the matched-filter receiver, optimum detection with adjacent-cell interference treated as Gaussian noise, the linear MMSE receiver, and a detector that performs MMSE-based successive interference cancellation for intracell users with linear MMSE processing of out-of-cell interference (assuming the codebooks of out-of-cell users are unknown at the receiver, while their signatures and channels states are known and used by the receiver for interference mitigation). Employing Gaussian codebooks, which conforms with the capacity achieving statistics, the latter receiver is equivalent in terms of spectral efficiency to optimum receiver under the constraints of single-cell-site processing, and that the transmissions of out-of-cell users cannot be decoded. The impact of taking into account the structure of multiuser interference at the receiver is clearly demonstrated in [14] and [15], as reflected by the spectral efficiencies of the above four receivers, differing in the amount and type of information available to the receiver with respect to other-users interference.

In this report, one step further is taken and the impact of employing *joint multiple-cell-site processing* on the performance randomly spread DS-CDMA systems is explored. Adhering again to Wyner's infinite linear cell-array model, it is assumed that the infinite array is divided into M-cells clusters. The receiver jointly processes the signals received at each of the cell-sites within the cluster, assuming that the signatures and codebooks of all intra-cluster users are available to the receiver. As for out-of-cluster users whose signals are received by the cluster's cell-sites, it is assumed that their codebooks are *unknown* to the receiver. The receiver is only aware of their signatures and uses this information for interference mitigation. Note that according to Wyner's model only the two neighboring cells outside the two edges of the M-cells cluster affect the receiver. Full channel state information is assumed available to the receiver for both intra- and out-of-cluster trans-

missions. It is worth mentioning here that the particular case of $M = 1$ boils down to *single-cell-site processing* [14], [15].

Binary spreading sequences are assumed and a variant of the flat-fading channel model analyzed in [6] and [15] is considered, focusing on Rayleigh fading. Unlike the common flat-fading model, it is assumed that a long *chip-level* interleaver is incorporated in each user's transmitter, and that a matching de-interleaver is incorporated in the corresponding multiple-cell receiver. The idea is to interleave, prior to transmission, chips corresponding to the spreading sequences of different channel symbols, in a way that, effectively, at the output of the de-interleaver at the receiver different chips experience independent fades, corresponding to a homogenous fading model [5] (commonly, as e.g. in [6] and [15], a *symbol-level* interleaver is assumed, and chips within the same spreading sequence experience the *same* channel fade).

Two types of receivers are considered:

(1). The *optimum* joint processor that achieves the mutual information between the channel input due to intra-cluster users and the M cell-site received signals, while accounting for the structure of the interference generated by out-of-cluster users;

(2). The linear MMSE receiver, that knows the signatures of all interfering users (both intra-cluster users and interfering users in adjacent clusters), and mitigates their interference by means of a linear MMSE filter. The outputs of the linear MMSE filter are then followed by single-user decoders.

The two receivers are analyzed and compared in terms of the cluster-averaged per-cell spectral efficiency, taken as the figure of merit for system performance. The key tool for the analysis is the observation that system model in concern is completely equivalent to a certain class of *multiple-input multiple-output* (MIMO) channel models. It is well known that degrees of freedom can be equivalently provided by the processing gain in a spread-spectrum system, or by the number of antenna elements in a system with an antenna array. Hence, results obtained for MIMO channels can be directly applied to the problem in concern. With that in mind, recently obtained results by Tulino et al in [16] are employed. In [16] the capacity of a rather general class of *single-user* MIMO channels is derived while assuming asymptotic conditions in terms of the number of both receiver and transmitter antennas (arguing that the results are well representative of systems with

a finite and practical number of antennas). Tulino et al also derive the achievable rate with a linear MMSE receiver, and identify an elegant relation between this rate and the maximum achievable rate, in an analogous manner to the relation shown in [6] (for a single-cell randomly spread single-cell DS-CDMA system). Appropriately interpreting the different quantities of [16], expressions for the per-cell spectral efficiencies of both the optimum and linear MMSE receiver are derived. The results are compared to previously obtained *single*-cell-site processing results [14], and the performance enhancement due to multiple-cell-site processing is demonstrated. The low- and high-SNR spectral efficiency slopes are investigated as well.

For the sake of comparison, and towards a more complete treatment of the multiple-cell-site processing problem, two modified multi-cell models are also considered. The first of the two models retains the linear cell-array structure, but assumes only the existence of M cluster-cells, the received signals of which are to be processed by the multiple-cell-site receiver. Thus, only intra-cluster multiuser interference is present, and the system model is referred to as the model of "isolated cells". This model leads to a somewhat simpler MIMO channel model interpretation, and is used to demonstrate the effect of other-cluster interference, assumed undecodable by the multiple-cell-site receiver, on system performance. It should be noted here that the model of "isolated cluster" is the complete analogy to the model considered in [11] and [13], where the signals received at all cell-sites were assumed to be processed by the joint multiple-cell-site processor, but in contrast to the current setting no random-spreading was employed. Here, the particular case of $M = 1$ boils down to the setting of a single isolated cell with homogenous fading, equivalent to the one analyzed in [5].

The second modified model considered in this report is a model in which the system cells form a *cirular* array, obtained by simply assuming that the first and the M-th cluster-cells are adjacent to each other. The circular structure of the resulting equivalent MIMO channel interpretation leads to particularly simple expressions for the spectral efficiency of both the optimum and linear MMSE receivers. To be more specific, the expressions are identical to those obtained for a single-cell system, as considered in [5], but where the average received power (SNR) of each user equals the sum of the average received power at its local cell-site plus the average received power at the two adjacent cell-sites (according to the Wyner model). Furthermore, as the analysis to follow shows, the average per-cell

spectral efficiencies in the two *linear* system models approach, as the cluster size M grows, the corresponding spectral efficiencies obtained in the circular array model. Hence, the circular array is a useful model for providing insight into the effect of joint multiple-cell-site processing, when the cluster of cells to be jointly processed is large enough (numerical results show that one can get very close to the circular array limit even for relatively moderate cluster sizes).

The last part of this report is devoted to the investigation of the impact of chip-level interleaving on system performance, while mainly confining the discussion to the optimum joint-multiple-cell-site receiver. At first, focusing on the circular-array model described above, two upper bounds on the performance of the optimum receiver with *symbol-level* interleaving are derived (one based on the Jensen bound, and a second tighter bound based on information theoretic arguments). It is then shown that the spectral efficiency of the optimum receiver with *chip-level* interleaving coincides with the above two upper bounds when the cell load is taken to infinity (which is also the optimum choice in terms of spectral efficiency for the optimum receiver in the circular-array setup). This result establishes the superiority of chip-level interleaving over symbol-level interleaving in the high cell load regime. Next, following Verdú [17], the minimum $\frac{E_b}{N_0}$ that enables reliable communications, and the low-SNR spectral efficiency slope of the optimum receiver is derived for the cases in which chip-level and symbol-level interleavers are employed, and also for the corresponding *non-fading* setup. Comparison of the three low-SNR spectral efficiencies shows that the spectral efficiency for the optimum receiver in a chip-level interleaved system (with flat fading) is higher than the corresponding slopes in both a symbol-interleaved system, and in the non-fading setup. Comparing the two latter slopes, the analysis also identifies the conditions (in terms of cell load and inter-cell interference factor values) in which flat-fading becomes beneficial in the low-SNR regime.

In order to get additional insight into the effect of chip-level interleaving, a single cell microdiversity multi-antenna setup, as considered in [10] and [6], is also investigated. Expressions for the spectral efficiencies of the optimum receiver and the linear MMSE receiver are derived, as well as their low- and high-SNR spectral efficiency slopes. The analysis shows, again, that the spectral efficiency attained with chip-level interleaving always upper bounds the one attained with symbol-level interleaving in extreme SNR and in the high cell load regimes. In view of the above results (for both the circular array

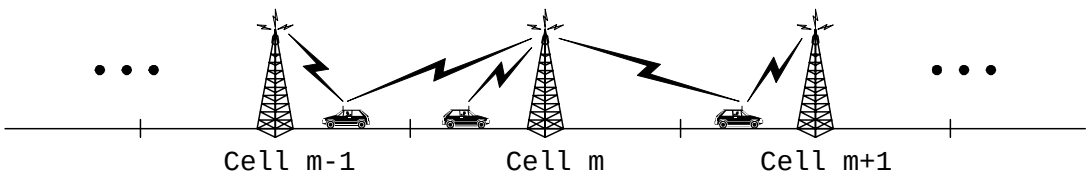

Figure 1: Wyner's infinite linear cell-array model.

and multi-antenna setups) it is therefore conjectured that the superiority of chip-level interleaving holds in general.

The structure of the this report is as follows. Section 2 presents the system model. Section 3 is devoted to a review of the main results of [16], and the equivalent MIMO interpretation. Next, the isolated cluster model is considered in Section 4, where expressions for the spectral efficiency of the optimum and linear MMSE receivers are presented. Section 5 and 6 follow with an analogous treatment of the infinite cell-array and circular array models. Section 7 includes numerical results and compares the three multi-cell models, respectively. Section 8 investigated the impact of chip-level interleaving on system performance. Finally, Section 9 ends this report with a summary and some concluding remarks.

2 System Model

Denoting by K the number of users per cell, and by N the length of the spreading sequences (the "processing gain"), the focus is on the asymptotic setup in which $K, N \to \infty$, while $K/N \to \beta < \infty$. As mentioned in the introduction, the constant β is commonly referred to as the "cell load". Adhering to Wyner's linear cell-array model, as depicted in Fig. 1, the baseband representation of the complex N-dimensional received signal vector at the m-th cell-site, at some arbitrary time index, is given by

$$\boldsymbol{y}_m = \alpha \boldsymbol{S}_{m-1} \circ \boldsymbol{H}_{m,m-1} \boldsymbol{x}_{m-1} + \boldsymbol{S}_m \circ \boldsymbol{H}_{m,m} \boldsymbol{x}_m + \alpha \boldsymbol{S}_{m+1} \circ \boldsymbol{H}_{m,m+1} \boldsymbol{x}_{m+1} + \boldsymbol{n}_m \quad , \quad (2\text{-}1)$$

where $\circ$ stands for the Hadamard product, defined for arbitrary matrices $\boldsymbol{A}$ and $\boldsymbol{B}$ as

$$[\boldsymbol{A} \circ \boldsymbol{B}]_{i,j} \triangleq [A]_{i,j}[B]_{i,j} \quad . \tag{2-2}$$

In the above notation bold lower case denotes vectors and bold upper case denotes matrices. The K-dimensional vector $\boldsymbol{x}_m$ consists of the symbols transmitted by the K users operating in the m-th cell. The users are assumed to employ Gaussian codebooks (which conforms with the capacity achieving statistics), and it is also assumed that the users cannot cooperate their transmissions in any way. Full channel state information is assumed to be available to the multiple cell-site receiver, however the users are assumed to be unaware of the instantaneous channel realizations. Therefore, the symbols transmitted by each of the users are assumed to be zero-mean i.i.d. (across time and users) circularly symmetric (proper) complex Gaussian random variables [18], with variance $\bar{P}$, that designates the equal transmit power of all users. The entries of the $N \times K$ matrices $\{\boldsymbol{H}_{m,n}\}$ are the channel chip-level fades affecting the signals transmitted by users in the n-th cell, *as observed by the m-th cell-site receiver*. With the underlying chip-level interleaver assumption, the entries of $\boldsymbol{H}_{m,n}$ matrices are taken as i.i.d. zero-mean circularly symmetric complex Gaussian random variables, with unit variance (corresponding to Rayleigh fading). The matrices are also assumed to be statistically independent for different values of m and n. The $N \times K$ matrices $\{\boldsymbol{S}_m\}$ denote the signature matrices, with the columns of the matrix $\boldsymbol{S}_m$ being the spreading sequences of the users operating in the m-th cell. It is assumed that the users employ random *binary* spreading sequences, so that the entries of the signature matrices are assumed to be i.i.d. random variables taking the values $\{-1/N, 1/N\}$ with equal probability. Independence of the spreading sequences of different users is also assumed. The underlying assumption of full channel state information at the receiver implies that the channel fade matrices $\{\boldsymbol{H}_{m,n}\}$ and the signature matrices $\{\boldsymbol{S}_m\}$ are instantaneously known at the receiver. Finally, the N-dimensional vector $\boldsymbol{n}_m$ denotes the additive white Gaussian noise (AWGN) at the receiver of the m-th cell-site, i.e., $\boldsymbol{n}_m$ is a zero mean circularly symmetric complex Gaussian random vector with $E\{\boldsymbol{n}_m \boldsymbol{n}_m{}^{\dagger}\} = \boldsymbol{I}_N$, where $\boldsymbol{I}_N$ denotes the $N \times N$ identity matrix. As can be observed the noise spectral level is normalized, without loss of generality, to unity, and thus $\bar{P}$ denotes, in fact, the signal-to-noise ratio of each of the users. The noise vectors at the receivers of different cell-sites are assumed to be i.i.d.

3 Preliminaries and Multi-Input Multi-Output Interpretation

As already mentioned in the introduction, the key tool used in the analysis to follow is a recent result by Tulino et al obtained for MIMO channels in [16] (see also [19] for an extensive review of results from the theory of random matrices and their applications to wireless communications). This section is devoted to a review of the main results of [16]. The manner in which the results can be applied to the multi-cell randomly spread DS-CDMA setup analyzed in this report, shall be made clear in the sections to follow, while indicating the proper interpretation of the main parameters of [16].

Consider now a system with n_T transmit and n_R receive antennas. Assuming frequency-flat fading, the corresponding channel model is

$$\boldsymbol{y} = \sqrt{g}\boldsymbol{H}\boldsymbol{x} + \boldsymbol{n} \quad , \tag{3-1}$$

where $\boldsymbol{x}$ and $\boldsymbol{y}$ are the n_T-dimensional transmit and n_R-dimensional received complex signal vectors, and $\boldsymbol{n}$ is a circularly symmetric complex Gaussian n_R-dimensional noise vector, with one-sided spectral density $N_0 = E\left\{\|\boldsymbol{n}\|^2\right\}/n_R$. The scalar g is a normalization factor, and the $n_R \times n_T$ channel transfer matrix $\boldsymbol{H}$ is assumed to be a zero-mean complex Gaussian matrix, the power of whose entries can be assembled into a matrix $\boldsymbol{P}$. The entries $[\boldsymbol{P}]_{i,j}$ of the matrix $\boldsymbol{P}$ are defined as $[\boldsymbol{P}]_{i,j} \triangleq E\left\{\left|[\boldsymbol{H}]_{i,j}^2\right|\right\}$, and the matrix is constrained to satisfy

$$\sum_{j=1}^{n_T}\sum_{i=1}^{n_R}[\boldsymbol{P}]_{i,j} = n_T n_R \quad . \tag{3-2}$$

The focus in [16] is on the asymptotic setup in which $n_T, n_R \to \infty$, while $n_T/n_R \to \beta < \infty$, and the aim is to derive the limiting ergodic capacity per receive antenna

$$C = \frac{1}{n_R}E\left\{\log\det\left(\boldsymbol{I} + \frac{\mathsf{SNR}}{n_T}\boldsymbol{H}\boldsymbol{H}^\dagger\right)\right\} \quad , \tag{3-3}$$

where the expectation is taken over the different channel realizations, and SNR, the average

signal-to-noise ratio, is defined through

$$\mathsf{SNR} = g\frac{E\left\{\|\boldsymbol{x}\|^2\right\}}{N_0} \quad . \tag{3-4}$$

Defining the *power profile*

$$\mathcal{P}^{(n_R)}(r,t) \triangleq [\boldsymbol{P}]_{i,j} \quad ; \quad \frac{i}{n_R} \le r < \frac{i+1}{n_R} \ , \ \frac{j}{n_T} \le t < \frac{j+1}{n_T} \ , \tag{3-5}$$

it is assumed that as the system dimensions grow large the above power profile converges uniformly to a bounded function

$$\mathcal{P}(r,t) \triangleq \lim_{\substack{n_R,n_T\to\infty \\ \frac{n_T}{n_R}\to\beta<\infty}} \mathcal{P}^{(n_R)}(r,t), \quad r\in(0,1],\ t\in(0,\beta] \quad , \tag{3-6}$$

referred to as the *asymptotic power profile*. With the above definitions and notation we can now quote the main result of [16].

Theorem 3.1 ([16], Proposition 1) *Consider a normalized channel $\boldsymbol{H}$ with uncorrelated entries and asymptotic power profile $\mathcal{P}$. The capacity per receive antenna converges, as $n_R, n_T \to \infty$, $\frac{n_T}{n_R} \to \beta < \infty$, to*

$$\begin{aligned} C(\beta,\mathsf{SNR}) = {} & \beta E\left\{\log(1+\mathsf{SNR}\,\Gamma(T,\mathsf{SNR}))\right\} + E\left\{\log(1+E\left\{\mathcal{P}(R,T)\Upsilon(T,\mathsf{SNR})\,|\,R\right\})\right\} \\ & - \beta E\left\{\Gamma(T,\mathsf{SNR})\Upsilon(T,\mathsf{SNR})\right\}\log e \quad , \end{aligned} \tag{3-7}$$

where the expectations are with respect to the random variables R and T, independent and uniformly distributed in $[0,1]$ and $[0,\beta]$, respectively, and with

$$\begin{aligned} \Gamma(t,\mathsf{SNR}) &= \frac{1}{\beta}E\left\{\frac{\mathcal{P}(R,t)}{1+E\left\{\mathcal{P}(R,T)\Upsilon(T,\mathsf{SNR})\,|\,R\right\}}\right\} \\ \Upsilon(t,\mathsf{SNR}) &= \frac{\mathsf{SNR}}{1+\mathsf{SNR}\,\Gamma(t,\mathsf{SNR})} \quad . \end{aligned} \tag{3-8}$$

It is noted that $\mathsf{SNR}\,\Gamma(t,\mathsf{SNR})$ represents the asymptotic signal-to-interference-plus-noise ratio (SINR) at the output of a linear MMSE receiver, as a function of the normalized antenna index t. Also, the mean-squared error at the output of such a receiver equals

$\Upsilon(t, \mathsf{SNR})/\mathsf{SNR}$.

The tradeoffs between power and bandwidth may be evaluated by expressing the capacity as a function of the normalized transmit or receive energy per bit

$$\begin{aligned} \frac{E_b^t}{N_0} &= \frac{\mathsf{SNR}}{C(\mathsf{SNR})} \\ \frac{E_b^r}{N_0} &= \frac{E_b^t}{N_0} g n_R \quad . \end{aligned} \tag{3-9}$$

It is also useful to approximate the capacity per receive antenna as a first order function of the energy per bit at the low- and high-SNR regimes [6] [17]. At the low-SNR regime the key performance measures are the minimum receive or transmit energy per bit required for reliable communication,

$$\begin{aligned} \frac{E_b^r}{N_{0\,\min}} &= \log_e 2 \\ \frac{E_b^t}{N_{0\,\min}} &= \frac{\log_e 2}{g n_R} \quad , \end{aligned} \tag{3-10}$$

and S_0, the low-SNR capacity per receive antenna slope in bits/sec/Hz/(3dB) [17]

$$S_0 = \frac{2 n_T^2 n_R}{\sum_{j=1}^{n_T} P_T^2(j) + \sum_{i=1}^{n_R} P_R^2(i)} \quad . \tag{3-11}$$

In (3-11) the total normalized power injected into the channel by the j-th antenna is defined as

$$P_T(j) \triangleq \sum_{i=1}^{n_R} [\boldsymbol{P}]_{i,j} \quad , \tag{3-12}$$

and the total normalized power collected by the i-th receive antenna is defined as

$$P_R(i) \triangleq \sum_{j=1}^{n_T} [\boldsymbol{P}]_{i,j} \quad . \tag{3-13}$$

At the high-SNR regime the key performance measure is the capacity per receive antenna high-SNR slope in bits/sec/Hz/(3dB) [6]

$$S_\infty \triangleq \frac{1}{n_R} \min(n_R', n_T') \quad , \tag{3-14}$$

where n_R' is the number of receive antennas for which $P_R(i) > 0$, and n_T' is the number of

transmit antennas for which $P_T(j) > 0$.

When the matrix $\boldsymbol{P}$ exhibits certain structures then the result of Theorem 3.1 can be significantly simplified. In particular, it can be shown [19] that if the matrix $\boldsymbol{P}$ is *asymptotically doubly regular*, then the result of Theorem 3.1 boils down to the function derived in [5] for independent identically distributed channels (with the appropriate scaling for complex channels). An $m \times n$ matrix $\boldsymbol{A}$ is *asymptotically row-regular* if for all i and $\xi \in \mathbb{R}$

$$\lim_{m\to\infty} \frac{1}{m} \sum_{j=1}^{m} 1\left\{[\boldsymbol{A}]_{i,j} < \xi\right\} \quad , \tag{3-15}$$

is independent of i. The matrix $\boldsymbol{A}$ is *asymptotically column-regular* if $\boldsymbol{A}^T$ is asymptotically row-regular, and it is asymptotically doubly-regular if it is asymptotically both row- and column-regular. Such a matrix satisfies

$$\lim_{m\to\infty} \frac{1}{m} \sum_{j=1}^{m} [\boldsymbol{A}]_{i,j} = \lim_{n\to\infty} \frac{1}{n} \sum_{i=1}^{n} [\boldsymbol{A}]_{i,j} \quad .$$

4 Isolated Cluster Setup

In this section we consider a single isolated cluster of M cells ordered in a linear array. The received signal in each cell-site is given by (2-1), except for the two cell-sites at the cluster edges (i.e. cell-sites 1 and M), as no cells outside the M-cells cluster are assumed. The notation $(\cdot)^{IC}$ shall be used to denote quantities related to this isolated cluster model. Unless stated otherwise all the derivations in this section are valid for $M \geq 2$. The overall received signal, as seen by the joint multiple-cell-site receiver, can be written in the following form

$$\boldsymbol{y}_{1\ [MN\times 1]}^{M} = \boldsymbol{S}_{[MN\times MK]}^{IC} \boldsymbol{x}_{1\ [MK\times 1]}^{M} + \boldsymbol{n}_{1\ [MN\times 1]}^{M} \quad , \tag{4-1}$$

where $\boldsymbol{y}_1^M = [\boldsymbol{y}_1^T, \ldots, \boldsymbol{y}_M^T]^T$, $\boldsymbol{x}_1^M = [\boldsymbol{x}_1^T, \ldots, \boldsymbol{x}_M^T]^T$, $\boldsymbol{n}_1^M = [\boldsymbol{n}_1^T, \ldots, \boldsymbol{n}_M^T]^T$, and the matrix $\boldsymbol{S}^{IC}$ equals

$$\boldsymbol{S}^{IC} = \begin{bmatrix} \boldsymbol{S}_1 \circ \boldsymbol{H}_{1,1} & \alpha \boldsymbol{S}_2 \circ \boldsymbol{H}_{1,2} & \mathbf{0} & \cdots & \mathbf{0} \\ \alpha \boldsymbol{S}_1 \circ \boldsymbol{H}_{2,1} & \boldsymbol{S}_2 \circ \boldsymbol{H}_{2,2} & \alpha \boldsymbol{S}_3 \circ \boldsymbol{H}_{2,3} & \mathbf{0} & \mathbf{0} \\ \mathbf{0} & \alpha \boldsymbol{S}_2 \circ \boldsymbol{H}_{3,2} & \boldsymbol{S}_3 \circ \boldsymbol{H}_{3,3} & \alpha \boldsymbol{S}_4 \circ \boldsymbol{H}_{3,4} & \cdots \\ & \ddots & \ddots & \ddots & \\ \mathbf{0} & \cdots & \mathbf{0} & \alpha \boldsymbol{S}_{M-1} \circ \boldsymbol{H}_{M,M-1} & \boldsymbol{S}_M \circ \boldsymbol{H}_{M,M} \end{bmatrix} . \tag{4-2}$$

The per-cell spectral efficiency of the *optimum* multiple cell-site processor in this setup is given by

$$C_{M\,\mathrm{opt}}^{IC} = \frac{1}{M} \lim_{\substack{N,K \to \infty \\ \frac{K}{N} \to \beta}} \frac{1}{N} E \left\{ \log \det \left(\boldsymbol{I} + \bar{P} \boldsymbol{S}^{IC} \boldsymbol{S}^{IC\dagger} \right) \right\} \quad . \tag{4-3}$$

Recall now the underlying assumption of binary spreading sequences, and independent circularly symmetric Gaussian channel fades, as described in Section 2. Under these assumptions, the entries of the channel transfer matrix $\boldsymbol{S}^{IC}$ are marginally Gaussian. Furthermore they are independent and hence jointly Gaussian (and uncorrelated). With this observation, we can now invoke the result of Theorem 3.1, and derive a more explicit expression for the spectral efficiency of (4-3). Comparing the latter expression to (3-3) the following correspondence between the single-user MIMO channel and the multi-cell DS-CDMA model is observed. The number of transmit antennas n_T is replaced by the total number of users MK, and the number of receive antennas is replaced by MN. Hence, the cell load β retains the same interpretation as in Theorem 3.1, i.e.,

$$\beta = \lim_{n_R \to \infty} \frac{n_T}{n_R} = \lim_{N \to \infty} \frac{K}{N} \quad . \tag{4-4}$$

Also, it is observed that the one-sided spectral density of the AWGN as in (3-1) satisfies $N_0 = 1$. Now in view of the channel transfer matrix power constraint of (3-2), it follows from (4-2) that

$$\sum_{i=1}^{MN} \sum_{i=1}^{MK} E \left\{ \left| [\boldsymbol{S}^{IC}]_{i,j} \right|^2 \right\} = [M + 2(M-1)\alpha^2] K \quad , \tag{4-5}$$

and forcing the relation $\sqrt{g^{IC}}\boldsymbol{H} = \boldsymbol{S}^{IC}$ we get

$$\begin{aligned} g^{IC} &= \frac{\left[M + 2(M-1)\alpha^2\right] K}{M^2 NK} \\ &= \left[1 + 2\alpha^2\left(1 - \frac{1}{M}\right)\right]\frac{1}{MN} \quad . \end{aligned} \tag{4-6}$$

Hence, the SNR as defined in (3-4) corresponds in the multi-cell DS-CDMA model to

$$\begin{aligned} \mathsf{SNR}^{IC} &\underset{N,K\to\infty,\frac{K}{N}\to\beta}{=} g^{IC} MK\bar{P} = g^{IC} MN\beta\bar{P} \\ &= \left[1 + 2\alpha^2\left(1 - \frac{1}{M}\right)\right]\beta\bar{P} \quad . \end{aligned} \tag{4-7}$$

Defining the *average per-user received SNR* as

$$\bar{P}_{av}^{IC} = \left[1 + 2\alpha^2\left(1 - \frac{1}{M}\right)\right]\bar{P} \quad , \tag{4-8}$$

where the average is taken over the M cell-site received signals, it is observed that $\mathsf{SNR}^{IC} = \beta\bar{P}_{av}^{IC}$. The final step towards applying Theorem 3.1 is to identify the asymptotic power profile of the channel in concern. Note that the power profile used in the Theorem corresponds to the matrix $\boldsymbol{H}$ in the single-user MIMO channel model of (3-1). Using the relation $\boldsymbol{H} = \frac{1}{\sqrt{g^{IC}}}\boldsymbol{S}^{IC}$ the resulting power profile is given by

$$[\boldsymbol{P}^{IC}]_{i,j} = \begin{cases} \frac{1}{g^{IC}N} \ , & \begin{pmatrix} (m-1)N+1 \le i \le mN \\ (m-1)K+1 \le j \le mK \end{pmatrix} \quad ; \quad m = 1,2,\ldots,M \\ \alpha^2\frac{1}{g^{IC}N} \ , & \begin{pmatrix} (m-1)N+1 \le i \le mN \\ mK+1 \le j \le (m+1)K \end{pmatrix} \quad ; \quad m = 1,2,\ldots,(M-1) \\ \alpha^2\frac{1}{g^{IC}N} \ , & \begin{pmatrix} mN+1 \le i \le (m+1)N \\ (m-1)K+1 \le j \le mK \end{pmatrix} \quad ; \quad m = 1,2,\ldots,(M-1) \\ 0 \ , & \text{Otherwise} \quad , \end{cases} \tag{4-9}$$

and it is easily verified that the constraint of (3-2) is satisfied and

$$\sum_{i=1}^{NM}\sum_{j=1}^{KM}[\boldsymbol{P}^{IC}]_{i,j} = M^2KN \quad . \tag{4-10}$$

The *asymptotic power profile* is now given by:

$$\mathcal{P}_M^{IC}(x,y) = \begin{cases} \frac{1}{g^{IC}N} \ , & \left(\begin{array}{c} \frac{(m-1)}{M} < x \leq \frac{m}{M} \\ \frac{(m-1)}{M}\beta < y \leq \frac{m}{M}\beta \end{array}\right) \quad ; \quad m = 1,2,\ldots,M \\ \alpha^2\frac{1}{g^{IC}N} \ , & \left(\begin{array}{c} \frac{(m-1)}{M} < x \leq \frac{m}{M} \\ \frac{m}{M}\beta < y \leq \frac{(m+1)}{M}\beta \end{array}\right) \quad ; \quad m = 1,2,\ldots,(M-1) \\ \alpha^2\frac{1}{g^{IC}N} \ , & \left(\begin{array}{c} \frac{m}{M} < x \leq \frac{(m+1)}{M} \\ \frac{(m-1)}{M}\beta < y \leq \frac{m}{M}\beta \end{array}\right) \quad ; \quad m = 1,2,\ldots,(M-1) \\ 0 \ , & \text{Otherwise} \quad , \end{cases} \tag{4-11}$$

where, $x \in (0,1]$ and $y \in (0,\beta]$.

Turning to (3-8), it follows that

$$\Gamma^{IC}(y,\mathsf{SNR}^{IC}) = \frac{1}{\beta}\int_0^1 \frac{\mathcal{P}_M^{IC}(x,y)}{1+\frac{1}{\beta}\int_0^\beta \frac{\mathcal{P}_M^{IC}(x,t)\mathsf{SNR}^{IC}}{1+\mathsf{SNR}^{IC}\Gamma^{IC}(t,\mathsf{SNR}^{IC})}\,dt}\,dx \quad . \tag{4-12}$$

Due to the particular structure of the asymptotic power profile, and the symmetry of intra-cell users (in each of the M cells), the function $\Gamma^{IC}(y,\mathsf{SNR}^{IC})$ can be written as a discrete function of the cell index m

$$\begin{aligned} \Gamma_M^{IC}(m) &= \frac{1}{\beta}\frac{1}{M}\sum_{l=1}^{M}\frac{\mathcal{P}_M^{IC}(l,m)}{1+\frac{1}{M}\sum_{k=1}^{M}\frac{\mathcal{P}_M^{IC}(l,k)\mathsf{SNR}^{IC}}{1+\mathsf{SNR}^{IC}\Gamma_M^{IC}(k)}} \\ &= \frac{1}{\beta}\frac{1}{M}\sum_{l=m-1}^{m+1}\frac{\mathcal{P}_M^{IC}(l,m)}{1+\frac{1}{M}\sum_{k=l-1}^{l+1}\frac{\mathcal{P}_M^{IC}(l,k)\mathsf{SNR}^{IC}}{1+\mathsf{SNR}^{IC}\Gamma_M^{IC}(k)}} \quad ; \quad m = 1,2,\cdots,M \quad , \end{aligned} \tag{4-13}$$

where the explicit dependency of Γ^{IC} in SNR^{IC} (or $\bar{P}$) was omitted for simplicity of notation.

Entries of negative indices within the sum expressions in (4-13) should be ignored, and

$$\mathcal{P}_M^{IC}(l,m) = \begin{cases} \frac{1}{g^{IC}N} \ , & m = l \\ \alpha^2 \frac{1}{g^{IC}N} \ , & |m-l| = 1 \\ 0 \ , & \text{Otherwise} \end{cases} \qquad (4\text{-}14)$$

$$m,\ l = 1, 2, \cdots, M \quad ,$$

The values of the function $\mathcal{P}_M^{IC}(l,m)$ correspond to the entries of $\frac{1}{g^{IC}N}\boldsymbol{\mathcal{P}}_M^{IC}$, where $\boldsymbol{\mathcal{P}}_M$ is the $M \times M$ Toeplitz matrix

$$\boldsymbol{\mathcal{P}}_M^{IC} = \begin{bmatrix} 1 & \alpha^2 & 0 & \cdots & 0 & 0 \\ \alpha^2 & 1 & \alpha^2 & 0 & \cdots & 0 \\ 0 & \alpha^2 & 1 & \alpha^2 & 0 & \ddots \\ \vdots & \ddots & \ddots & \ddots & \ddots & 0 \\ 0 & \cdots & 0 & \alpha^2 & 1 & \alpha^2 \\ 0 & 0 & \cdots & 0 & \alpha^2 & 1 \end{bmatrix} \quad . \qquad (4\text{-}15)$$

Rewriting (4-13) in terms of (4-15) yields

$$\begin{aligned} \Gamma_M^{IC}(m) &= \frac{1}{\beta}\frac{1}{M}\sum_{l=m-1}^{m+1} \frac{\mathcal{P}_M^{IC}(l,m)}{1 + \frac{1}{M}\sum_{k=l-1}^{l+1} \frac{\mathcal{P}_M^{IC}(l,k) g^{IC} MN\beta\bar{P}}{1+g^{IC}MN\beta\bar{P}\,\Gamma_M^{IC}(k)}} \\ &= \frac{1}{\beta}\left[1 + 2\alpha^2\left(1 - \frac{1}{M}\right)\right]^{-1} \sum_{l=m-1}^{m+1} \frac{[\boldsymbol{\mathcal{P}}_M^{IC}]_{l,m}}{1 + \sum_{k=l-1}^{l+1} \frac{[\boldsymbol{\mathcal{P}}_M^{IC}]_{l,k}\beta\bar{P}}{1+\Gamma_M^{IC}(k)\left[1+2\alpha^2\left(1-\frac{1}{M}\right)\right]\beta\bar{P}}} \end{aligned} \qquad (4\text{-}16)$$

$$m = 1, 2, \cdots, M \quad ,$$

where "out-of-range" indices should be ignored. Using the above definition of $\Gamma_M^{IC}(m)$ and (3-8) one gets

$$\Upsilon_M^{IC}(m) = \frac{\left[1 + 2\alpha^2\left(1 - \frac{1}{M}\right)\right]\beta\bar{P}}{1 + \Gamma_M^{IC}(m)\left[1 + 2\alpha^2\left(1 - \frac{1}{M}\right)\right]\beta\bar{P}} \quad , \qquad (4\text{-}17)$$

and following (3-7) the spectral efficiency of the optimum multiple cell-site processor is

given by

$$
\begin{aligned}
C^{IC}_{M\,\mathrm{opt}} = \beta\frac{1}{M}\sum_{m=1}^{M}\log\left(1+\Gamma^{IC}_{M}(m)\left[1+2\alpha^2\left(1-\frac{1}{M}\right)\right]\beta\bar{P}\right) \\
+\frac{1}{M}\sum_{m=1}^{M}\log\left(1+\left[1+2\alpha^2\left(1-\frac{1}{M}\right)\right]^{-1}\sum_{k=m-1}^{m+1}[\boldsymbol{\mathcal{P}}^{IC}_{M}]_{m,k}\Upsilon^{IC}_{M}(k)\right) \\
-\beta\frac{1}{M}\sum_{m=1}^{M}\Gamma^{IC}_{M}(m)\Upsilon^{IC}_{M}(m)\log e \quad .
\end{aligned}
\tag{4-18}
$$

Finally, substituting (4-17) into (4-18) gets

$$
\begin{aligned}
C^{IC}_{M\,\mathrm{opt}} = \frac{1}{M}\sum_{m=1}^{M}\beta\log\left(1+\Gamma^{IC}_{M}(m)\left[1+2\alpha^2\left(1-\frac{1}{M}\right)\right]\beta\bar{P}\right) \\
+\frac{1}{M}\sum_{m=1}^{M}\log\left(1+\sum_{k=m-1}^{m+1}\frac{[\boldsymbol{\mathcal{P}}^{IC}_{M}]_{m,k}\beta\bar{P}}{1+\Gamma^{IC}_{M}(k)\left[1+2\alpha^2\left(1-\frac{1}{M}\right)\right]\beta\bar{P}}\right) \\
-\frac{1}{M}\sum_{m=1}^{M}\beta\frac{\Gamma^{IC}_{M}(m)\left[1+2\alpha^2\left(1-\frac{1}{M}\right)\right]\beta\bar{P}}{1+\Gamma^{IC}_{M}(m)\left[1+2\alpha^2\left(1-\frac{1}{M}\right)\right]\beta\bar{P}}\log e \quad ,
\end{aligned}
\tag{4-19}
$$

or more compactly, using (4-8),

$$
\begin{aligned}
C^{IC}_{M\,\mathrm{opt}} = \frac{1}{M}\sum_{m=1}^{M}\beta\log\left(1+\Gamma^{IC}_{M}(m)\beta\bar{P}^{IC}_{av}\right) \\
+\frac{1}{M}\sum_{m=1}^{M}\log\left(1+\sum_{k=m-1}^{m+1}\frac{[\boldsymbol{\mathcal{P}}^{IC}_{M}]_{m,k}\beta\bar{P}}{1+\Gamma^{IC}_{M}(k)\beta\bar{P}^{IC}_{av}}\right) \\
-\frac{1}{M}\sum_{m=1}^{M}\beta\frac{\Gamma^{IC}_{M}(m)\beta\bar{P}^{IC}_{av}}{1+\Gamma^{IC}_{M}(m)\beta\bar{P}^{IC}_{av}}\log e \quad .
\end{aligned}
\tag{4-20}
$$

The per-cell spectral efficiency of the linear MMSE detector can be readily deduced from (4-20). In fact it is given by the first sum expression in (4-20), where each term of index m gives the spectral efficiency of the linear MMSE detector for the m-th cell. That is,

$$
C^{IC}_{M\,\mathrm{ms}} = \frac{1}{M}\sum_{m=1}^{M}\beta\log\left(1+\Gamma^{IC}_{M}(m)\beta\bar{P}^{IC}_{av}\right) \quad . \tag{4-21}
$$

It should be emphasized however that although each term in the sum refers to the contribution of a single-cell to the overall throughput, this contribution is achieved by using a *multiple-cell-site* linear processor, in contrast to the single-cell-site processor considered in [6] or [15].

Following are some basic properties of the two receivers in the isolated cluster model.

Proposition 4.1 *The minimum transmit and receive* $\frac{E_b}{N_0}$ *that enable reliable communications for both the optimum and linear MMSE receivers equal*

$$\begin{aligned} \frac{E_b^{r\,IC}}{N_0}_{min} &= \log_e 2 \\ \frac{E_b^{t\,IC}}{N_0}_{min} &= \frac{\log_e 2}{\left[1+2\alpha^2(1-\frac{1}{M})\right]} \quad . \end{aligned} \tag{4-22}$$

Proof: The result is immediately obtained from (3-10) and (4-6). ■

Proposition 4.2 *The low- and high-SNR spectral efficiency slopes of the optimum receiver are given by*

$$S_{0\ opt}^{IC} = \frac{2\beta}{1+\beta}\frac{\left[1+2\alpha^2(1-\frac{1}{M})\right]^2}{\left[1+4\alpha^2(1-\frac{1}{M})+4\alpha^4(1-\frac{3}{2M})\right]} \quad , \tag{4-23}$$

and

$$S_{\infty\ opt}^{IC} = \begin{cases} \beta\ , & \beta \le 1 \\ 1\ , & \beta > 1 \quad . \end{cases} \tag{4-24}$$

These results are valid for arbitrary values of K, N *and* $M \ge 2$.

Proof: The proof follows in a similar manner to proof of the corresponding results for the infinite array setup discussed in Section 5 (see App. B.2.1 and B.3). ■

The low-SNR slope monotonically increases with β, thus validating the optimality of increasing β without bound in the low-SNR regime. It is also interesting to see that for $M = 2$ (4-23) boils down to $2\beta/(1+\beta)$, which is the low-SNR slope achieved in a non-fading single-cell setup [6]. This result should come in no surprise while observing that the channel transfer matrix in the isolated cluster setup is in fact doubly-regular for $M = 2$ (see Section 3). The non-fading single-cell low-SNR slope is also obtained asymptotically as $M \to \infty$. In contrast, the high-SNR slope of (4-24) is identical to the slope obtained in the non-fading single-cell setup for all values of M.

Proposition 4.3 *The low-SNR spectral efficiency slope of the linear MMSE is given by*

$$S_{0\ ms}^{IC} = \frac{2\beta}{1+2\beta} \frac{\left[1+2\alpha^2\left(1-\frac{1}{M}\right)\right]^2}{\left[1+4\alpha^2\left(1-\frac{1}{M}\right)+4\alpha^4\left(1-\frac{3}{2M}\right)\right]} \quad ; \quad M \geq 2 \quad , \tag{4-25}$$

Proof: The proof follows in a similar manner to the corresponding proof in App. B.2.2. ■

Note that as for the optimum receiver, the low-SNR slope of the linear MMSE receiver reduces to the corresponding slope in single-cell non-fading setup $2\beta/(1+2\beta)$, when $M = 2$ and $M \to \infty$. Again, (4-25) demonstrates the optimality of increasing β without bound for the linear MMSE receiver in the low-SNR regime.

Proposition 4.4 *For $\beta \to \infty$ the spectral efficiency of the optimum receiver, $C_{M\ opt}^{IC}$, is given by the solution of the following implicit equation*

$$C_{M\ opt}^{IC} = \frac{(M-2)}{M} \log\left(1+\frac{1+2\alpha^2}{1+2\alpha^2\left(1-\frac{1}{M}\right)} C_{M\ opt}^{IC} \frac{E_b^r}{N_0}\right) + \frac{2}{M}\log\left(1+\frac{1+\alpha^2}{1+2\alpha^2\left(1-\frac{1}{M}\right)} C_{M\ opt}^{IC} \frac{E_b^r}{N_0}\right) \quad ; \quad M \geq 2 \quad . \tag{4-26}$$

Proof: The proof follows in a similar manner to corresponding proof in App. B.4.2. ■

Note that as the cluster size M grows, (4-26) coincides with the spectral efficiency in the non-fading single-cell setup [5], for which taking $\beta \to \infty$ is optimum for *all values* of $\frac{E_b}{N_0}$. Furthermore, for the particular case of $M = 2$ the limiting optimum spectral efficiency is given by

$$C_{2\ \text{opt}}^{IC} \underset{\beta\to\infty}{=} \log\left(1+C_{2\ \text{opt}}^{IC}\frac{E_b^r}{N_0}\right) \quad . \tag{4-27}$$

This result coincides with the the non-fading single-cell optimum spectral efficiency result due to the asymptotic double regularity property of the channel transfer matrix for $M = 2$.

Proposition 4.5 *For $\beta \to \infty$, the spectral efficiency of the linear MMSE receiver, $C_{M\ ms}^{IC}$,*

is given by the solution of the following quadratic equation

$$\left(C^{IC}_{M\ ms}\right)^{\ 2} + C^{IC}_{M\ ms}\left[\frac{(2+3\alpha^2)\left[1+2\alpha^2\left(1-\frac{1}{M}\right)\right]}{(1+\alpha^2)(1+2\alpha^2)}\left(\frac{E_b^r}{N_0}\right)^{-1} - \log e\right] + \frac{\left[1+2\alpha^2\left(1-\frac{1}{M}\right)\right]^2}{(1+\alpha^2)(1+2\alpha^2)}\left(\frac{E_b^r}{N_0}\right)^{-1}\left[\left(\frac{E_b^r}{N_0}\right)^{-1} - \log e\right] = 0 \quad ; \quad M \geq 2 \quad . \quad (4\text{-}28)$$

Proof: The proof follows in a similar manner to corresponding proof in App. B.4.1. ■

As observed for the optimum receiver, for the particular case of $M = 2$, the solution of (4-28) coincides with the corresponding result in the single-cell non-fading setup

$$C^{IC}_{2\ \mathrm{ms}} \underset{\beta\to\infty}{=} \log e - \left(\frac{E_b^r}{N_0}\right)^{-1} \quad . \quad (4\text{-}29)$$

It is also observed from (4-28), that the linear MMSE receiver becomes interference limited for $\beta \to \infty$, and the spectral efficiency reaches the limit of $\log e$ as $\frac{E_b}{N_0}$ is increased without bound.

5 Infinite Linear Array Setup

This section focuses on the infinite linear array setup, as described in Section 1. The notation $(\cdot)^{IA}$ shall be used to denote quantities related to this model. Unless stated otherwise all the derivations in this section are valid for $M \geq 2$. Without any loss of generality the expressions to follow relate to the cluster of cells numbered $\{1, 2, \ldots, M\}$. The signal vector received by the joint multiple-cell-site receiver for the cluster in concern is given by

$$\boldsymbol{y}^{M}_{1\ [MN\times 1]} = \boldsymbol{S}^{IA}_{[MN\times(M+2)K]}\boldsymbol{x}^{M+1}_{0\ [(M+2)K\times 1]} + \boldsymbol{n}^{M}_{1\ [MN\times 1]} \quad , \quad (5\text{-}1)$$

where, $\boldsymbol{y}_1^M = [\boldsymbol{y}_1^T, \boldsymbol{y}_2^T, \ldots, \boldsymbol{y}_M^T]^T$, $\boldsymbol{x}_0^{M+1} = [\boldsymbol{x}_0^T, \boldsymbol{x}_1^T, \ldots, \boldsymbol{x}_M^T, \boldsymbol{x}_{M+1}^T]^T$, and $\boldsymbol{n}_1^M = [\boldsymbol{n}_1^T, \boldsymbol{n}_2^T, \ldots, \boldsymbol{n}_M^T]^T$. The $MN \times (M+2)K$ channel transfer matrix $\boldsymbol{S}^{IA}$ equals,

$$\boldsymbol{S}^{IA} = \begin{bmatrix} \alpha \boldsymbol{S}_0 \circ \boldsymbol{H}_{1,0} & & \boldsymbol{0} \\ \boldsymbol{0} & & \boldsymbol{0} \\ \vdots & \boldsymbol{S}^{IC} & \vdots \\ \boldsymbol{0} & & \boldsymbol{0} \\ \boldsymbol{0} & & \alpha \boldsymbol{S}_{M+1} \circ \boldsymbol{H}_{M,M+1} \end{bmatrix} \quad , \tag{5-2}$$

where $\boldsymbol{S}^{IC}$ is the $MN \times MK$ channel transfer matrix of the isolated cluster setup, as defined in (4-2).

The spectral efficiency of the optimum receiver in this setting is given by

$$C_{M\,\mathrm{opt}}^{IA} = \frac{1}{M} \lim_{\substack{N,K \to \infty \\ \frac{K}{N} \to \beta}} \frac{1}{N} E\left\{ I(\boldsymbol{x}_1, \ldots, \boldsymbol{x}_M \,;\, \boldsymbol{y}_1, \ldots, \boldsymbol{y}_M) \right\} \quad , \tag{5-3}$$

where one has to bare in mind, in contrast to the isolated cluster setup, that the cell-sites at the edges of the M-cells cluster receive signals from users of adjacent clusters (see (5-1)). According to the underlying assumptions of the current setting, these other-cluster transmissions cannot be decoded by the receiver, which is only aware of the structure of their signals. Using Kolmogorov's identity, the mutual information in (5-3) can be rewritten as

$$I\left(\boldsymbol{x}_1^M \,;\, \boldsymbol{y}_1^M\right) = I\left(\boldsymbol{x}_0^{M+1} \,;\, \boldsymbol{y}_1^M\right) - I\left(\boldsymbol{x}_0, \boldsymbol{x}_{M+1} \,;\, \boldsymbol{y}_1^M \,|\, \boldsymbol{x}_1^M\right) \quad . \tag{5-4}$$

Due to the underlying assumptions of the Wyner model, the second expression in the righthand side (RHS) of (5-4) can be written for $M \geq 2$ as

$$\begin{aligned} I\left(\boldsymbol{x}_0, \boldsymbol{x}_{M+1} \,;\, \boldsymbol{y}_1^M \,|\, \boldsymbol{x}_1^M\right) &= I\left(\boldsymbol{x}_0, \boldsymbol{x}_{M+1} \,;\, \boldsymbol{y}_1, \boldsymbol{y}_M \,|\, \boldsymbol{x}_1^M\right) \\ &= I\left(\boldsymbol{x}_0 \,;\, \boldsymbol{y}_1 \,|\, \boldsymbol{x}_1, \boldsymbol{x}_2\right) + I\left(\boldsymbol{x}_{M+1} \,;\, \boldsymbol{y}_M \,|\, \boldsymbol{x}_{M-1}, \boldsymbol{x}_M\right) \\ &= 2I\left(\boldsymbol{x}_0 \,;\, \boldsymbol{y}_1 \,|\, \boldsymbol{x}_1, \boldsymbol{x}_2\right) \quad , \end{aligned} \tag{5-5}$$

where the last equality follows from the symmetry between the two cells at the edges of the cluster. Substituting (5-4) and (5-5) into (5-3), the spectral efficiency of the optimum

receiver is given by

$$C^{IA}_{M\,\mathrm{opt}} = \mathcal{C}_M - \frac{2}{M}\mathcal{C}_I \quad , \tag{5-6}$$

where

$$\begin{aligned} \mathcal{C}_M &\triangleq \frac{1}{M} \lim_{\substack{N,K\to\infty \\ \frac{K}{N}\to\beta}} \frac{1}{N} E\left\{ I\left(\boldsymbol{x}_0^{M+1}\,;\,\boldsymbol{y}_1^{M}\right)\right\} \\ &= \frac{1}{M} \lim_{\substack{N,K\to\infty \\ \frac{K}{N}\to\beta}} \frac{1}{N} E\left\{ \log\det\left(\boldsymbol{I} + \bar{P}\boldsymbol{S}^{IA}\boldsymbol{S}^{IA\dagger}\right)\right\} \quad , \end{aligned} \tag{5-7}$$

and

$$\begin{aligned} \mathcal{C}_I &\triangleq \lim_{\substack{N,K\to\infty \\ \frac{K}{N}\to\beta}} \frac{1}{N} E\left\{ I\left(\boldsymbol{x}_0\,;\,\boldsymbol{y}_1 \,|\, \boldsymbol{x}_1, \boldsymbol{x}_2\right)\right\} \\ &= \lim_{\substack{N,K\to\infty \\ \frac{K}{N}\to\beta}} \frac{1}{N} E\left\{ \log\det\left(\boldsymbol{I} + \alpha^2\bar{P}\boldsymbol{S}^{I}\boldsymbol{S}^{I\dagger}\right)\right\} \quad . \end{aligned} \tag{5-8}$$

The $N \times K$ matrix $\boldsymbol{S}^I$ in (5-8) is the channel transfer matrix corresponding to users of cell 0, whose signals are received at cell-site 1, given by

$$\boldsymbol{S}^I \triangleq \boldsymbol{S}_0 \circ \boldsymbol{H}_{1,0} \quad . \tag{5-9}$$

Examining (5-6), it is observed that $\mathcal{C}_M$ can be interpreted as the average per-cell spectral efficiency in the case in which the receiver also tries to decode the transmissions of users in the two cluster-adjacent cells (assuming that their codebooks are now also known at the receiver). That is, the setup corresponds to an extended cluster of $(M+2)$ cells, consisting of the original cluster of M cells and the two cluster-adjacent cells (cells 0 and $(M+1)$), while only the signals received at the M cells-sites of the original cluster are being processed by the receiver. The quantity $\mathcal{C}_I$ may be interpreted as the spectral efficiency of an optimum receiver in a single isolated cell setup with homogenous fading [5], and with a scaled SNR of $\alpha^2\bar{P}$.

Observing (5-7) and (5-8), the same argumentation of Section 4 regarding the entries of $\boldsymbol{S}^{IA}$ and $\boldsymbol{S}^I$ can be used to conclude that the channel interpretations corresponding to $\mathcal{C}_M$ and $\mathcal{C}_I$ both fit the framework of Theorem 3.1. Starting with $\mathcal{C}_M$, and in order to properly use the results of Theorem 3.1, a new parameter $\tilde{\beta}$, interpreted as the system average cell

load, is defined as

$$\tilde{\beta} \triangleq \lim_{n_R \to \infty} \frac{n_T}{n_R} = \lim_{N,K \to \infty} \frac{(M+2)K}{MN} = \frac{M+2}{M}\,\beta \quad . \tag{5-10}$$

The channel transfer matrix power constraint of (3-2) translates for (5-2) to

$$\sum_{i=1}^{K(M+2)} \sum_{j=1}^{NM} E\left\{ \left| \left[\boldsymbol{S}^{IA} \right]_{i,j} \right|^2 \right\} = (1+2\alpha^2)MK \quad . \tag{5-11}$$

Hence, in view of (3-1) and (3-4) it follows that

$$g^{IA} = \frac{[1+2\alpha^2]\,MK}{M(M+2)KN} = (1+2\alpha^2)\frac{1}{(M+2)N} \quad , \tag{5-12}$$

and

$$\begin{aligned} \mathsf{SNR}^{IA} \underset{N,K\to\infty,\frac{K}{N}\to\beta}{=} g^{IA}(M+2)K\bar{P} \; &= g^{IA}MN\tilde{\beta}\bar{P} \\ &= (1+2\alpha^2)\frac{M}{M+2}\tilde{\beta}\bar{P} \\ &= (1+2\alpha^2)\beta\bar{P} \quad . \end{aligned} \tag{5-13}$$

The *average per-user received SNR* is defined as

$$\bar{P}_{av}^{IA} = \frac{M}{M+2}(1+2\alpha^2)\bar{P} \quad . \tag{5-14}$$

Following the procedure used in Section 4, the discrete-index asymptotic power profile $\mathcal{P}_M^{IA}(l,m)$ is defined, corresponding to the entries of $\frac{1}{g^{IA}N}\boldsymbol{\mathcal{P}}_M^{IA}$, where $\boldsymbol{\mathcal{P}}_M^{IA}$ is the following $M \times (M+2)$ matrix

$$\boldsymbol{\mathcal{P}}_M^{IA} = \begin{bmatrix} \alpha^2 & 1 & \alpha^2 & 0 & \cdots & & 0 \\ 0 & \alpha^2 & 1 & \alpha^2 & 0 & \cdots & 0 \\ \vdots & \ddots & \ddots & \ddots & \ddots & \ddots & \vdots \\ 0 & 0 & \cdots & 0 & \alpha^2 & 1 & \alpha^2 \end{bmatrix} \quad . \tag{5-15}$$

For convenience, and in order to match between the matrix indices and the cell indices, the rows of $\boldsymbol{\mathcal{P}}_M^{IA}$ are enumerated $l = \{1,\ldots,M\}$, while the columns are enumerated $m = \{0,\ldots,(M+1)\}$. Accordingly, the values of the discrete-index function $\Gamma_M^{IA}(m)$ are given

by the unique solutions to the following set of equations

$$\begin{aligned}
\Gamma_M^{IA}(m) &= \frac{1}{\tilde{\beta}}\frac{1}{M}\sum_{l=m-1}^{m+1}\frac{\mathcal{P}_M^{IA}(l,m)}{1+\frac{1}{M+2}\sum_{k=l-1}^{l+1}\frac{\mathcal{P}_M^{IA}(l,k)\mathsf{SNR}^{IA}}{1+\mathsf{SNR}^{IA}\Gamma_M^{IA}(k)}} \\
&= \frac{1}{\tilde{\beta}}\frac{1}{M}\sum_{l=m-1}^{m+1}\frac{\mathcal{P}_M^{IA}(l,m)}{1+\frac{1}{M+2}\sum_{k=l-1}^{l+1}\frac{\mathcal{P}_M^{IA}(l,k)g^{IA}MN\tilde{\beta}\bar{P}}{1+g^{IA}MN\tilde{\beta}\bar{P}\Gamma_M^{IA}(k)}} \\
&= \frac{1}{\tilde{\beta}}\frac{M+2}{M}\left(1+2\alpha^2\right)^{-1}\sum_{l=m-1}^{m+1}\frac{[\boldsymbol{\mathcal{P}}_M^{IA}]_{l,m}}{1+\frac{M}{M+2}\sum_{k=l-1}^{l+1}\frac{[\boldsymbol{\mathcal{P}}_M^{IA}]_{l,k}\tilde{\beta}\bar{P}}{1+\Gamma_M^{IA}(k)(1+2\alpha^2)\frac{M}{M+2}\tilde{\beta}\bar{P}}} \\
&= \frac{1}{\beta}\left(1+2\alpha^2\right)^{-1}\sum_{l=m-1}^{m+1}\frac{[\boldsymbol{\mathcal{P}}_M^{IA}]_{l,m}}{1+\sum_{k=l-1}^{l+1}\frac{[\boldsymbol{\mathcal{P}}_M^{IA}]_{l,k}\beta\bar{P}}{1+\Gamma_M^{IA}(k)(1+2\alpha^2)\beta\bar{P}}} \\
&\qquad\qquad m=0,1,\ldots,M+1 \quad ,
\end{aligned} \tag{5-16}$$

where "out-of-range" indices should be ignored. In addition, it follows from (3-8) and (5-12) that

$$\begin{aligned}
\Upsilon_M^{IA}(m) &= \frac{(1+2\alpha^2)\frac{M}{M+2}\tilde{\beta}\bar{P}}{1+\Gamma_M^{IA}(m)(1+2\alpha^2)\frac{M}{M+2}\tilde{\beta}\bar{P}} \\
&= \frac{(1+2\alpha^2)\beta\bar{P}}{1+\Gamma_M^{IA}(m)(1+2\alpha^2)\beta\bar{P}} \quad .
\end{aligned} \tag{5-17}$$

Finally, combining (3-7), (5-16) and (5-17),

$$\begin{aligned}
\mathcal{C}_M =& \frac{1}{M+2}\sum_{m=0}^{M+1}\tilde{\beta}\log\left(1+\Gamma_M^{IA}(m)(1+2\alpha^2)\frac{M}{M+2}\tilde{\beta}\bar{P}\right) \\
&+\frac{1}{M}\sum_{m=1}^{M}\log\left(1+\frac{M}{M+2}\sum_{k=m-1}^{m+1}\frac{[\boldsymbol{\mathcal{P}}_M^{IA}]_{m,k}\tilde{\beta}\bar{P}}{1+\Gamma_M^{IA}(k)(1+2\alpha^2)\frac{M}{M+2}\tilde{\beta}\bar{P}}\right) \\
&-\frac{1}{M+2}\sum_{m=0}^{M+1}\tilde{\beta}\frac{\Gamma_M^{IA}(m)(1+2\alpha^2)\frac{M}{M+2}\tilde{\beta}\bar{P}}{1+\Gamma_M^{IA}(m)(1+2\alpha^2)\frac{M}{M+2}\tilde{\beta}\bar{P}}\log e \quad ,
\end{aligned} \tag{5-18}$$

or more compactly

$$\begin{aligned}\mathcal{C}_M =&\frac{1}{M+2}\sum_{m=0}^{M+1}\tilde{\beta}\log\left(1+\Gamma_M^{IA}(m)\tilde{\beta}\bar{P}_{av}^{IA}\right)\\&+\frac{1}{M}\sum_{m=1}^{M}\log\left(1+\frac{M}{M+2}\sum_{k=m-1}^{m+1}\frac{[\boldsymbol{\mathcal{P}}_M^{IA}]_{m,k}\tilde{\beta}\bar{P}}{1+\Gamma_M^{IA}(k)\tilde{\beta}\bar{P}_{av}^{IA}}\right)\\&-\frac{1}{M+2}\sum_{m=0}^{M+1}\tilde{\beta}\frac{\Gamma_M^{IA}(m)\tilde{\beta}\bar{P}_{av}^{IA}}{1+\Gamma_M^{IA}(m)\tilde{\beta}\bar{P}_{av}^{IA}}\log e\quad .\end{aligned}\tag{5-19}$$

Alternatively, expressing (5-18) in terms of the cell-load β yields

$$\begin{aligned}\mathcal{C}_M =&\frac{1}{M}\sum_{m=0}^{M+1}\beta\log\left(1+\Gamma_M^{IA}(m)(1+2\alpha^2)\beta\bar{P}\right)\\&+\frac{1}{M}\sum_{m=1}^{M}\log\left(1+\sum_{k=m-1}^{m+1}\frac{[\boldsymbol{\mathcal{P}}_M^{IA}]_{m,k}\beta\bar{P}}{1+\Gamma_M^{IA}(k)(1+2\alpha^2)\beta\bar{P}}\right)\\&-\frac{1}{M}\sum_{m=0}^{M+1}\beta\frac{\Gamma_M^{IA}(m)(1+2\alpha^2)\beta\bar{P}}{1+\Gamma_M^{IA}(m)(1+2\alpha^2)\beta\bar{P}}\log e\quad .\end{aligned}\tag{5-20}$$

In order to complete the derivation of the spectral efficiency of the optimum receiver, it remains to derive an expression for $\mathcal{C}_I$. However with the single-cell interpretation discussed above, (5-8) can be interpreted as the spectral efficiency of the optimum receiver in a single-cell setup with homogeneous *Rayleigh* flat fading [6] and an equivalent transmit power of $\alpha^2\bar{P}$. Accordingly, C_I is explicitly given by

$$\mathcal{C}_I=\beta\log\left(1+\alpha^2\bar{P}-\frac{1}{4}\mathcal{F}(\alpha^2\bar{P},\beta)\right)+\log\left(1+\alpha^2\bar{P}\beta-\frac{1}{4}\mathcal{F}(\alpha^2\bar{P},\beta)\right)-\frac{\log e}{4\alpha^2\bar{P}}\mathcal{F}(\alpha^2\bar{P},\beta)\,.\tag{5-21}$$

Turning to the linear MMSE receiver, then under the assumption of Gaussian codebooks, its average per-cell spectral efficiency equals

$$C_{M\,\mathrm{ms}}^{IA}\triangleq\frac{1}{M}\sum_{m=1}^{M}\lim_{\substack{N,K\to\infty\\ \frac{K}{N}\to\beta}}\sum_{k=1}^{K}\frac{1}{N}E\left\{I\left(x_{m,k}\;;\;\boldsymbol{y}_1^M\right)\right\}\quad .\tag{5-22}$$

According to [16], the quantity $\Gamma_M^{IA}(m)\mathsf{SNR}^{IA}=\Gamma_M^{IA}(m)\left(1+2\alpha^2\right)\beta\bar{P}$ is recognized as the

SINR at the output of the joint multi-cell linear MMSE receiver for users of the m-th intra-cluster cell. Hence, the average per-cell spectral efficiency of the linear MMSE receiver is given by

$$C_{M\,\mathrm{ms}}^{IA} = \frac{1}{M}\sum_{m=1}^{M} \beta \log\left(1+\Gamma_M^{IA}(m)(1+2\alpha^2)\beta\bar{P}\right) \quad . \tag{5-23}$$

Note that although the cluster receiver processes the signals of users from $M+2$ cells (M intra-cluster cells and the two cluster-adjacent cells), the average in (5-23) is over intra-cluster cells only, as codebooks of out-of-cluster users are assumed to be unknown at the receiver.

The following propositions present some basic properties of the two receivers in the infinite linear array setup.

Proposition 5.1 *The minimum transmit and receive $\frac{E_b}{N_0}$ that enable reliable communications for both the optimum and linear MMSE receivers equal*

$$\begin{aligned} \frac{E_b^r}{N_0}_{min}^{IA} &= \log_e 2 \\ \frac{E_b^t}{N_0}_{min}^{IA} &= \frac{\log_e 2}{\left[1+2\alpha^2\left(1-\frac{1}{M}\right)\right]} \quad . \end{aligned} \tag{5-24}$$

Proof: See App. B.1. ■

Proposition 5.2 *The low- and high-SNR spectral efficiency slopes of the optimum receiver are given by*

$$S_{0_{opt}}^{IA} = \frac{2\beta}{1+\beta}\frac{\left[1+2\alpha^2(1-\frac{1}{M})\right]^2}{\left[1+4\alpha^2\left(1-\frac{1}{(1+\beta)M}\right)+4\alpha^4\left(1-\frac{(3+\beta)}{2(1+\beta)M}\right)\right]} \quad , \tag{5-25}$$

and

$$S_{\infty\ opt}^{IA} = \begin{cases} \beta\ , & \beta \le \frac{M}{M+2} \\ 1-\frac{2}{M}\beta\ , & \frac{M}{M+2} < \beta \le 1 \\ 1-\frac{2}{M}\ , & 1 \le \beta \quad . \end{cases} \tag{5-26}$$

These results are valid for arbitrary values of K, N and $M \ge 2$.

Proof: See Apps. B.2.1 and B.3 for the low- and high-SNR spectral efficiency slopes of

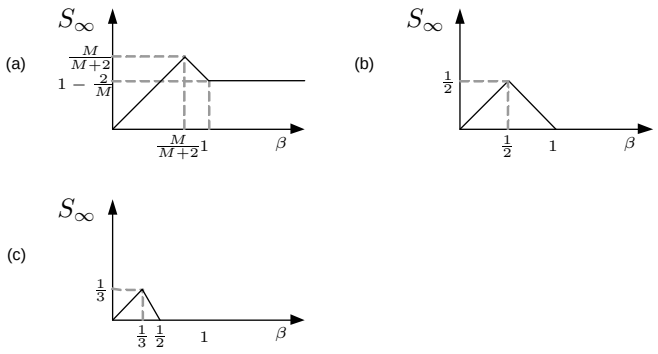

Figure 2: $S^{IA}_{\infty\,\mathrm{opt}}$ as a function of β for (a) $M > 2$, (b) $M = 2$, and (c) $M = 1$.

the optimum receiver, respectively. ■

As can be observed, (5-25) is the product of the low-SNR slope of the spectral efficiency of the optimum receiver in the single-cell non-fading setup [6] (i.e., $2\beta/(1+\beta)$), and a term that goes to unity as the cluster size M grows. It is also observed that (5-25) monotonically increases with the cell load β, thus establishing the optimality of increasing β without bound for the optimum receiver in the low-SNR regime. The limiting slope as $\beta \to \infty$ is given by

$$\lim_{\beta\to\infty} S^{IA}_{0_{\mathrm{opt}}} = \frac{2\left[1+2\alpha^2\left(1-\frac{1}{M}\right)\right]^2}{(1+2\alpha^2)^2-\frac{2\alpha^2}{M}} \quad . \tag{5-27}$$

The high-SNR spectral efficiency slope of the optimum receiver is depicted as a function of the cell load β in Fig. 2. Examining the high-SNR slope it is observed that taking $\beta \to \infty$ is no longer optimum in this regime. In fact the optimum value of β in terms of the high-SNR slope approaches $\frac{M}{M+2}$ as $\frac{E_b}{N_0} \to \infty$. It is interesting to note that when $M = 1$ [15], taking $\beta \to \infty$ turns the receiver *interference limited*, that is its spectral efficiency goes to a limit as $\frac{E_b}{N_0} \to \infty$. This behavior is also observed for $M = 2$ (joint two cell-site processing). In contrast, it is observed that for $M \geq 3$ the receiver is no longer interference limited when $\beta \to \infty$, although as said above, this is a strictly suboptimum choice for the cell-load in the high SNR regime.

Proposition 5.3 *The low-SNR spectral efficiency slope of the linear MMSE receiver is*

given by

$$S_{0_{ms}}^{IA} = \frac{2\beta}{1+2\beta} \frac{\left[1+2\alpha^2(1-\frac{1}{M})\right]^2}{\left[1+4\alpha^2\left(1-\frac{1+\beta}{(1+2\beta)M}\right)+4\alpha^4\left(1-\frac{3+4\beta}{(1+2\beta)M}\right)\right]} \quad ; \quad M \geq 2 \quad . \tag{5-28}$$

Proof: See App. B.2.2. ■

Note that as was the case for the optimum receiver, the low SNR slope of the linear MMSE receiver also coincides, as the cluster size M grows, with the corresponding slope in the single-cell non-fading setup, i.e., $2\beta/(1+2\beta)$ [6]. The slope of (5-28) monotonically increases with β to a limiting slope of

$$\lim_{\beta\to\infty} S_{0_{\rm ms}}^{IA} = \frac{\left[1+2\alpha^2(1-\frac{1}{M})\right]^2}{(1+2\alpha^2)^2 - \frac{2\alpha^2}{M}(1+4\alpha^2)} \quad , \tag{5-29}$$

which again establishes the optimality of taking $\beta \to \infty$ for the linear MMSE receiver in the low SNR regime, as shown for the optimum receiver.

Proposition 5.4 *For $\beta \to \infty$, the spectral efficiency of the optimum receiver, $C_{M\ opt}^{IA}$, is given by the solution of the following implicit equation*

$$C_{M\ opt}^{IA} = \log\left(1+\frac{(1+2\alpha^2)}{\left[1+2\alpha^2\left(1-\frac{1}{M}\right)\right]}\frac{E_b^r}{N_0}C_{M\ opt}^{IA}\right) - \frac{2}{M}\log\left(1+\frac{\alpha^2}{\left[1+2\alpha^2\left(1-\frac{1}{M}\right)\right]}\frac{E_b^r}{N_0}C_{M\ opt}^{IA}\right) \quad ; \quad M \geq 2 \quad . \tag{5-30}$$

Proof: See App. B.4.2. ■

As can be observed, as the cluster size M grows, (5-30) coincides with the spectral efficiency in the non-fading single-cell setup [5], for which taking $\beta \to \infty$ is optimum for *all values* of $\frac{E_b}{N_0}$.

Proposition 5.5 *For $\beta \to \infty$, the spectral efficiency of the linear MMSE receiver is given by*

$$C_{M\ ms}^{IA} = \frac{\left[1+2\alpha^2\left(1-\frac{1}{M}\right)\right]}{(1+2\alpha^2)}\left(\log e - \left(\frac{E_b^r}{N_0}\right)^{-1}\right) \quad ; \quad M \geq 2 \quad . \tag{5-31}$$

Proof: See App. B.4.1. ■

Note that the last term in (5-31) equals the spectral efficiency of the linear MMSE receiver in the single-cell non-fading setup (for $\beta \to \infty$), and the two results coincide as $M \to \infty$. Also, the MMSE receiver becomes *interference limited* for $\beta \to \infty$, and as $\frac{E_b^r}{N_0} \to \infty$ the spectral efficiency approaches the limit of

$$C_{M\,\mathrm{ms}}^{IA} \underset{\beta, \frac{E_b^r}{N_0} \to \infty}{=} \frac{\left[1 + 2\alpha^2\left(1 - \frac{1}{M}\right)\right]}{(1 + 2\alpha^2)} \log e \quad . \tag{5-32}$$

6 Circular Array Setup

In this section a slight modification is made to the original Wyner linear array setup, as described in Section 2, and analyzed in Section 4. It is now assumed that the M system cells are arranged in a *circle*, so that the first cell and the M-th cell are adjacent to one another (with $M \geq 3$). As shall be evident in the sequel, this modified structure has an inherent (circular) symmetry that leads to simple analytical results. Furthermore, the circular model becomes particularly useful, as it will be shown in the following that as $M \to \infty$ the spectral efficiency results for the isolated cluster and the infinite linear array setups coincide with those of the circular array setup. The notation $(\cdot)^C$ shall be used to denote quantities related to the circular array setting.

The overall received signal, as seen by the joint multiple-cell-site receiver, can be described by (4-1), while replacing the channel transfer matrix $\boldsymbol{S}^{IC}$ by

$$\boldsymbol{S}^C = \begin{bmatrix} \boldsymbol{S}_1 \circ \boldsymbol{H}_{1,1} & \alpha \boldsymbol{S}_2 \circ \boldsymbol{H}_{1,2} & \mathbf{0} & \cdots & \alpha \boldsymbol{S}_M \circ \boldsymbol{H}_{1,M} \\ \alpha \boldsymbol{S}_1 \circ \boldsymbol{H}_{2,1} & \boldsymbol{S}_2 \circ \boldsymbol{H}_{2,2} & \alpha \boldsymbol{S}_3 \circ \boldsymbol{H}_{2,3} & \cdots & \mathbf{0} \\ \mathbf{0} & \alpha \boldsymbol{S}_2 \circ \boldsymbol{H}_{3,2} & \boldsymbol{S}_3 \circ \boldsymbol{H}_{3,3} & \alpha \boldsymbol{S}_4 \circ \boldsymbol{H}_{3,4} & \cdots \\ & \ddots & \ddots & \ddots & \\ \alpha \boldsymbol{S}_1 \circ \boldsymbol{H}_{M,1} & \mathbf{0} & \cdots & \alpha \boldsymbol{S}_{M-1} \circ \boldsymbol{H}_{M,M-1} & \boldsymbol{S}_M \circ \boldsymbol{H}_{M,M} \end{bmatrix} . \tag{6-1}$$

In this framework the cell load β retains the same interpretation as in Theorem 3.1. Forcing

the relation $\sqrt{g^C}\boldsymbol{H} = \boldsymbol{S}^C$ yields

$$\begin{aligned} g^C &= \frac{M\left[1+2\alpha^2\right]K}{M^2NK} \\ &= \left(1+2\alpha^2\right)\frac{1}{MN} \quad , \end{aligned} \tag{6-2}$$

and the SNR as defined in (3-4) corresponds in the circular array setup to

$$\begin{aligned} \mathsf{SNR}^C \underset{N,K\to\infty,\,\frac{K}{N}\to\beta}{=} g^C MK\bar{P} &= g^C MN\beta\bar{P} \\ &= (1+2\alpha^2)\beta\bar{P} \quad . \end{aligned} \tag{6-3}$$

The average per-user received SNR in the circular array setup is simply

$$\bar{P}_{av}^C = \left(1+2\alpha^2\right)\bar{P} \quad . \tag{6-4}$$

The spectral efficiency is derived in an analogous manner to Section 4. Due to the circular nature of the channel, the discrete-index asymptotic power profile (cf. (4-14)) is given by $\frac{1}{g^C N}\boldsymbol{\mathcal{P}}_M^C$, where $\boldsymbol{\mathcal{P}}_M^C$ is the $M \times M$ *circular* matrix

$$\boldsymbol{\mathcal{P}}_M^C = \begin{bmatrix} 1 & \alpha^2 & 0 & \cdots & 0 & \alpha^2 \\ \alpha^2 & 1 & \alpha^2 & 0 & \cdots & 0 \\ 0 & \alpha^2 & 1 & \alpha^2 & 0 & \ddots \\ \vdots & \ddots & \ddots & \ddots & \ddots & 0 \\ 0 & \cdots & 0 & \alpha^2 & 1 & \alpha^2 \\ \alpha^2 & 0 & \cdots & 0 & \alpha^2 & 1 \end{bmatrix} \quad . \tag{6-5}$$

Hence, due to the circular symmetry and in contrast to the *linear* array discussed in Section 4, it is straightforward to see that the solution to the equation corresponding to (4-13) in the current setting, the discrete-index function $\Gamma_M^C(m)$, is independent of the choice of the cell index m within the circular array. Furthermore, since $\bar{P}_{av}^C$ is not a function of M, $\Gamma_M^C(m)$ is also independent of the size of the circular array M, and thus $\Gamma_M^C(m) = \Gamma^C,\ m = 1, \ldots, M$. Applying the latter observation to (4-13), Γ^C is given by the unique solution to the following

reduced equation

$$\Gamma^C = \frac{1}{\beta}\frac{1}{1+\frac{\beta\bar{P}_{av}^C}{1+\Gamma^C\beta\bar{P}_{av}^C}} \quad , \tag{6-6}$$

or

$$\beta\Gamma^C + \beta\frac{\beta\Gamma^C\bar{P}_{av}^C}{1+\Gamma^C\beta\bar{P}_{av}^C} = 1 \quad . \tag{6-7}$$

Equation (6-7) is a quadratic equation for Γ^C for which an explicit analytical solution can be obtained:

$$\Gamma^C = \frac{1}{\beta}\left[\frac{1-\beta}{2} - \frac{1}{2\bar{P}_{av}^C} + \sqrt{\frac{(1-\beta)^2}{4} + \frac{1+\beta}{2\bar{P}_{av}^C} + \frac{1}{4\bar{P}_{av}^{C\,2}}}\right] \quad . \tag{6-8}$$

Finally, using the symmetry argumentation, (6-7), and in analogy to equation (4-20) it is concluded that the spectral efficiency of the optimum receiver is given by

$$C_{\text{opt}}^C = \beta\log(1+\beta\Gamma^C\bar{P}_{av}^C) + \log\frac{1}{\beta\Gamma^C} + (\beta\Gamma^C - 1)\log e \quad , \tag{6-9}$$

and that the spectral efficiency of the linear MMSE receiver is given by

$$C_{\text{ms}}^C = \beta\log(1+\beta\Gamma^C\bar{P}_{av}^C) \quad . \tag{6-10}$$

Examining (6-7)-(6-10), it is observed that the results of the circular array setup are identical to the results of the non-fading (equivalently homogenous fading) single-cell setup [5], but with an increased average transmit power per user satisfying $\bar{P}_{av} = (1+2\alpha^2)\bar{P}$. Joint multiple cell-site processing is thus observed to completely eliminate the effect of other-cell interference while fully exploiting the total received power from each user, as received by the antennas of three cell-sites according to Wyner's model. Using the above equivalence the spectral efficiency of the optimum receiver can be more explicitly expressed as [5]

$$C_{\text{opt}}^C = \beta\log\left[1+\bar{P}_{av}^C - \frac{1}{4}\mathcal{F}(\bar{P}_{av}^C,\beta)\right] + \log\left[1+\bar{P}_{av}^C\beta - \frac{1}{4}\mathcal{F}(\bar{P}_{av}^C,\beta)\right] - \frac{\log e}{4\bar{P}_{av}^C}\mathcal{F}(\bar{P}_{av}^C,\beta) \quad , \tag{6-11}$$

where

$$\mathcal{F}(x,z) \triangleq \left(\sqrt{x\left(1+\sqrt{z}\right)^2+1} - \sqrt{x\left(1-\sqrt{z}\right)^2+1}\,\right)^2 \quad . \tag{6-12}$$

It is noted that the above results can also be obtained immediately by observing that the power profile matrix of $\boldsymbol{S}^C$ is asymptotically doubly-regular (see Section 3), and Proposition 3 of [16] can be used to obtain (6-7)-(6-10).

Using (3-10) and (6-2), the minimum $\frac{E_b}{N_0}$ required for reliable communication in the circular setup is given by

$$\begin{aligned} \frac{E_b^r}{N_0}^C_{\min} &= \log_e 2 \\ \frac{E_b^t}{N_0}^C_{\min} &= \frac{\log_e 2}{(1+2\alpha^2)} \quad . \end{aligned} \tag{6-13}$$

Taking $\beta \to \infty$, and expressing the spectral efficiency of the linear MMSE receiver in terms of the received $\frac{E_b}{N_0}$ yields

$$C^C_{\text{ms}} = \log e - \left(\frac{E_b^r}{N_0}\right)^{-1} \quad . \tag{6-14}$$

For the optimum receiver it can be shown that the spectral efficiency for $\beta \to \infty$ is given by

$$C^C_{\text{opt}} = \log\left(1 + C^C_{\text{opt}} \frac{E_b^r}{N_0}\right) \quad . \tag{6-15}$$

As can be observed the above result coincides with the spectral efficiency of the single-user AWGN channel. Furthermore, this result coincides with the result of [13] for the setup in which no random spreading is employed, demonstrating thus the optimality of taking $\beta \to \infty$ for the optimum receiver.

To obtain the low- and high-SNR spectral efficiency slopes of the optimum receiver, one can directly apply the single-cell results of [6] yielding

$$S^C_{0\ \text{opt}} = \frac{2\beta}{1+\beta} \quad , \tag{6-16}$$

and

$$S^C_{\infty_{\text{opt}}} = \begin{cases} \beta, & \beta \leq 1 \\ 1\ , & \beta > 1 \end{cases} \quad . \tag{6-17}$$

The optimality of increasing β without bound is clearly evident from the fact that both slopes monotonically increase with β. The low-SNR slope for the linear MMSE receiver is given by [6]

$$S^C_{0\ \text{ms}} = \frac{2\beta}{1+2\beta} \quad , \tag{6-18}$$

demonstrating the optimal choice of $\beta \to \infty$ for the linear MMSE receiver at the low-SNR regime. The high-SNR slope of the linear MMSE receiver is given by

$$S^{C}_{\infty_{\mathrm{ms}}} = \begin{cases} \beta \ , & \beta < 1 \\ 1/2 \ , & \beta = 1 \\ 0 \ , & \beta > 1 \end{cases} \quad . \tag{6-19}$$

The following Theorem defines the relation between the spectral efficiencies of optimum receiver in the multi-cell setups considered in this report.

Theorem 6.1

$$\lim_{M\to\infty} C^{IC}_{M\ opt} = \lim_{M\to\infty} C^{IA}_{M\ opt} = C^{C}_{opt} \quad . \tag{6-20}$$

Proof: See App. A. ■

It is noted that the coincidence of the minimum $\frac{E_b}{N_0}$ that enables reliable communications, and of the low- and high-SNR slopes in the three setups, as $M \to \infty$, can also be observed from the explicit expressions of these quantities as derived in Sections 4 and 5.

7 Numerical Results

In this section we bring some numerical results that demonstrate the performance enhancement of joint multiple-cell-site processing, and the inter-relations between the three multi-cell setups considered in this report. Figures 3 and 4 show the spectral efficiencies in the infinite array setup of the optimum receiver (5-6), and the linear MMSE receiver (5-23), respectively. The spectral efficiencies are plotted as a function of the transmit $\frac{E_b}{N_0}$ for the optimum choice of β (which is in general a function of $\frac{E_b}{N_0}$). The results were evaluated for $\alpha = \frac{1}{2}$, which corresponds to the case in which the total average inter-cell interference power equals one-half of the total average intra-cell received power, and can be considered as a "practical" level of inter-cell interference. As discussed above, while examining the low-SNR slope of the receivers, it is optimum for low values of $\frac{E_b}{N_0}$ to take $\beta \to \infty$. However, beyond some critical value of $\frac{E_b}{N_0}$ the optimum choice for β decreases from infinity and takes on finite values, approaching eventually, for the optimum receiver, the value of $M/(M+2)$ in the high-SNR regime. The region in which the optimum choice of

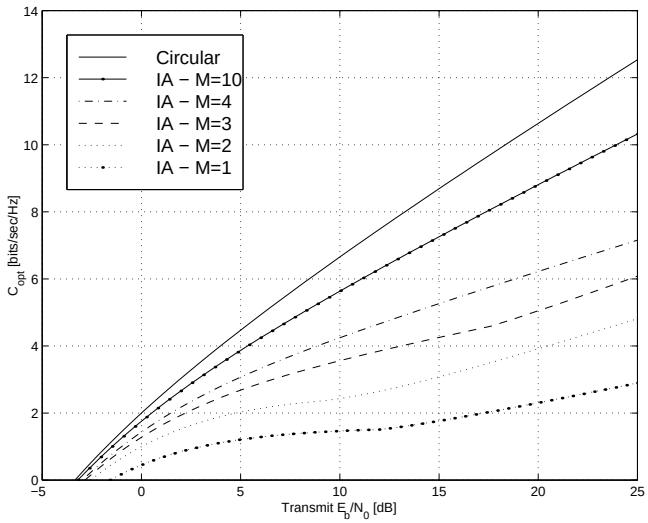

Figure 3: Spectral efficiency of the optimum receiver vs. transmit $\frac{E_b}{N_0}$ in the infinite linear array model, for $\alpha = 1/2$ and optimum choice of β.

β decreases from infinity explains the knee effect observed in the spectral efficiency curves for both receivers. The optimum values of β for the linear MMSE receiver are depicted in Fig. 5 as a function of $\frac{E_b^t}{N_0}$.

For the sake of comparison, we included in all figures the corresponding spectral efficiencies for the case of $M = 1$ [14], and for the circular array setup. Comparing the results, the dramatic effect of employing joint multiple cell-site processing on system performance is clearly evident. The approach of the spectral efficiency in the infinite linear cell-array setup to the spectral efficiency obtained in the circular array setup, as the cluster size M gets large, is also clearly observed for both receivers.

In order to emphasize the impact of joint multiple-cell-processing even further, Fig. 6 shows the average per-cell spectral efficiency of the joint multiple-cell-site linear MMSE receiver for $M = 2$ and $M = 3$, together with the spectral efficiencies obtained with *single*-cell-site processing ($M = 1$) of both the optimum and linear MMSE receivers [15]. The spectral efficiencies are plotted in Fig. 6 as a function of the transmit $\frac{E_b}{N_0}$ for the optimum choice of β, and for $\alpha = 1/2$. As can be observed, already with a joint 2-cell-site processor, the *linear* MMSE receiver outperforms the optimum single-cell-site processing receiver in the low $\frac{E_b}{N_0}$ regime, below some threshold $\frac{E_b}{N_0}$, and in the high $\frac{E_b}{N_0}$ region, beyond a threshold.

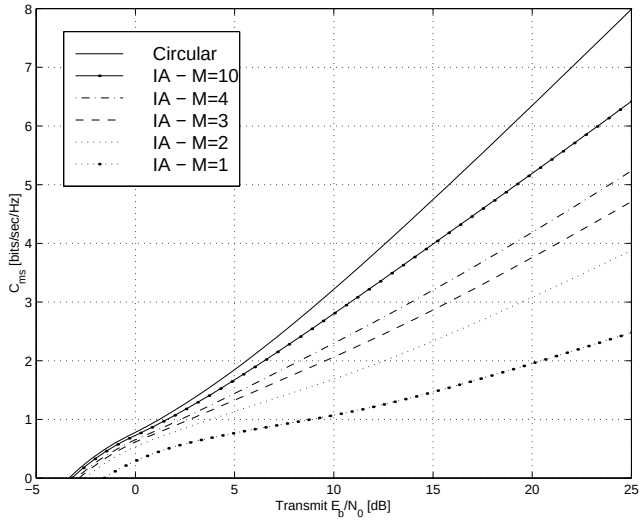

Figure 4: Spectral efficiency of the linear MMSE receiver vs. transmit $\frac{E_b}{N_0}$ in the infinite linear array model, for $\alpha = 1/2$ and optimum choice of β.

Furthermore, with no more than joint 3-cell-site processing, the linear MMSE receiver outperforms the optimum single-cell-site processing receiver for *all* values of $\frac{E_b}{N_0}$. This result is of particular practical interest in view of the fundamental receiver complexity difference between the two settings. The complexity of the optimum single-cell-site processing receiver grows *exponentially* with the number of users per cell, while that of the joint 3-cell linear MMSE receiver grows only *linearly* with the number of users per-cell.

To conclude, Figs. 7 and 8 show the average per-cell spectral efficiencies of the optimum and linear MMSE receivers, respectively, as a function of the transmit $\frac{E_b}{N_0}$, in the isolated cluster setup. Again, the spectral efficiencies are evaluated for the optimum choice of the cell load β, and for $\alpha = 1/2$. Comparing the results to the results obtained for the infinite array setup, as plotted in Figs. 3 and 4, it is immediately observed that, as the cluster size M grows the spectral efficiencies in the isolated cluster setup approach much faster the ones of the circular array setup, than those in the infinite array setup. In fact one gets very close to the asymptotic circular array results already when the cluster size equals $M = 3$. This clear difference between the two setups demonstrates the impact of undecodable inter-cell interference on system performance.

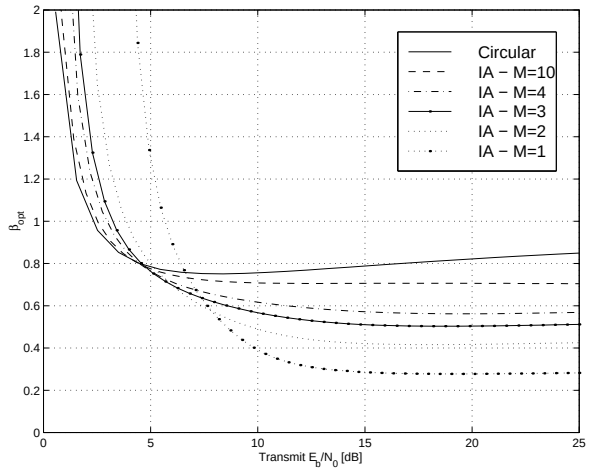

Figure 5: The optimum cell-load β for the linear MMSE receiver as function of the transmit $\frac{E_b}{N_0}$ model, for $\alpha = 1/2$.

8 The Impact of Chip-Level Interleaving

As discussed in the introduction to this report, incorporating a chip-level interleaver results in a homogenous fading process [6], in which each spreading chip of each user experiences independent fades. This comes in contrast to the conventional use of a symbol-level interleaver, resulting in a fading process in which the whole spreading sequence (N chips) of each user experiences the same fade, and the fades are independent from symbol to symbol. Hence, the terms homogeneous fading, and non-homogeneous fading, shall be used interchangeably in the following to refer to the chip-level interleaved and symbol-level interleaved setups, respectively. Most of this report is dedicated to the investigation of multi-cell setups employing chip-level interleaving, for which analytical results can be obtained following [16]. However, it is of great interest to compare these results to the ones obtained in the more practical multi-cell setups employing symbol-level interleavers.

When single-cell-site processing is employed, it is already well known from [5], [6], [14], and [15], that while homogenous fading has no effect on the spectral efficiency as compared to non-fading channels, flat-fading decreases the spectral efficiency of symbol-level interleaved systems (assuming no channel state information at the transmitter). Unfortunately, the derivation of the spectral efficiency with non-homogeneous fading in the *multi-cell* sys-

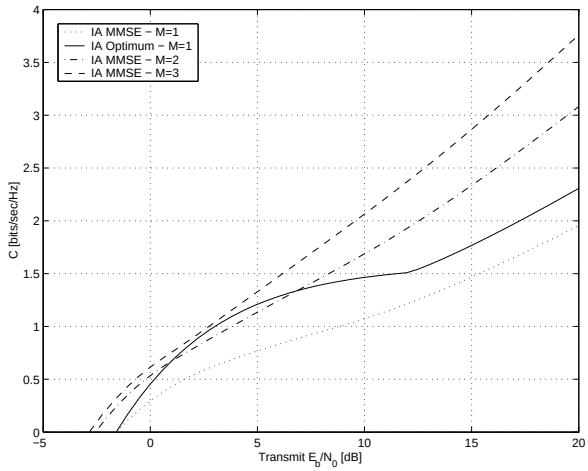

Figure 6: Comparison of joint multiple-cell-site linear MMSE processing and optimum single-cell-site processing, for the optimum choice of β and $\alpha = 1/2$.

tem setups considered in this report poses some considerable analytical difficulties, and is still an open problem. Therefore, in order to compare the two fading models, we focus on the optimum joint multiple-cell-site receiver and do the following. First, two bounding techniques are used to demonstrate the superiority of the optimum spectral efficiency obtained in the homogenous fading multi-cell model, in the high cell load region. Next, the low-SNR regime is considered for which the same behavior is also observed. Furthermore, it is proved that in the low-SNR regime fading may turn out beneficial, in terms of the optimum spectral efficiency, as compared to the corresponding setup in the absence of fading. This conclusion comes in contrast to the case of single-cell-site processing.

The above comparison is confined to the circular array setup of Section 6 (with the necessary adaptations to the non-homogeneous and non-faded setups), as it leads to more tractable results on one hand while capturing the impact of joint multiple-cell-site processing on the other. In addition, this model also provides a good approximation and an upper bound to the spectral efficiencies obtained in the more "realistic" infinite linear-array setup of Section 5, for rather moderate values of the cluster size M, as evident from the numerical results of Section 7. It is noted however, that the same analysis can be repeated for the infinite-array and isolated-cluster setups in a rather straightforward manner.

Finally, a multi-antenna model is investigated, which also demonstrates that homoge-

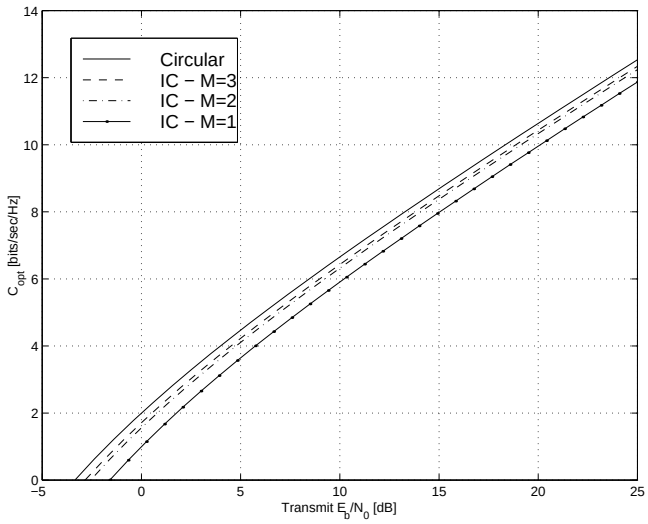

Figure 7: Spectral efficiency of the optimum detector vs. transmit $\frac{E_b}{N_0}$ in the isolated cells model, for $\alpha = 1/2$ and optimum choice of β.

nous fading can be beneficial in terms of the optimum spectral efficiency, as compared to non-homogeneous fading. The investigation considers several scenarios including the low- and high-SNR regimes, and the case in which the cell load is high.

The above investigations lead us to conjecture that homogeneous fading is beneficial in terms of the optimum spectral efficiency for all SNRs and cell load values.

8.1 Symbol-Interleaved System Model

Based on the general system model described in Section 2, and the circular array setup defined in Section 6, the overall received signal while employing symbol-level interleaving can be described by (4-1), while replacing the channel transfer matrix $\boldsymbol{S}^{IC}$ by

$$\boldsymbol{S}^{CS} = \begin{bmatrix} \boldsymbol{S}_1\boldsymbol{H}_{1,1} & \alpha\boldsymbol{S}_2\boldsymbol{H}_{1,2} & \boldsymbol{0} & \cdots & \alpha\boldsymbol{S}_M\boldsymbol{H}_{1,M} \\ \alpha\boldsymbol{S}_1\boldsymbol{H}_{2,1} & \boldsymbol{S}_2\boldsymbol{H}_{2,2} & \alpha\boldsymbol{S}_3\boldsymbol{H}_{2,3} & \cdots & \boldsymbol{0} \\ \boldsymbol{0} & \alpha\boldsymbol{S}_2\boldsymbol{H}_{3,2} & \boldsymbol{S}_3\boldsymbol{H}_{3,3} & \alpha\boldsymbol{S}_4\boldsymbol{H}_{3,4} & \cdots \\ & \ddots & \ddots & \ddots & \\ \alpha\boldsymbol{S}_1\boldsymbol{H}_{M,1} & \boldsymbol{0} & \cdots & \alpha\boldsymbol{S}_{M-1}\boldsymbol{H}_{M,M-1} & \boldsymbol{S}_M\boldsymbol{H}_{M,M} \end{bmatrix}. \quad (8\text{-}1)$$

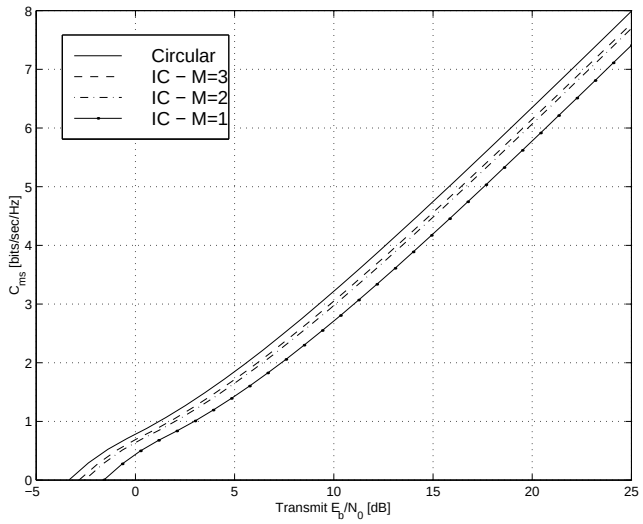

Figure 8: Spectral efficiency of the linear MMSE detector vs. transmit $\frac{E_b}{N_0}$ in the isolated cells model, for $\alpha = 1/2$ and optimum choice of β.

The notation $(\cdot)^{CS}$ shall be used to denote quantities related to the symbol-level interleaved setting. $\boldsymbol{S}_m$ in (8-1) denotes the binary $N \times K$ signature matrix of the K users of the m-th cell, and $\boldsymbol{H}_{n,m}$ denotes the $K \times K$ diagonal matrix of channel fades affecting the signals of the n-th cell users, when received at the m-th cell-site antenna. It is assumed that all channel fades are zero-mean, unit-variance i.i.d. random variables, and perfectly known to the receiver. Note, that when a chip-level interleaver is employed, the resulting fading process is mathematically described by the Hadamard multiplication of the signature matrix by the fading matrix. On the other hand, the use of a symbol-level interleaver yields a fading process that is described using conventional matrix multiplication of the signature matrix by the diagonal fading matrix.

8.2 High Cell Load Upper Bounds

8.2.1 Jensen Bound

For any N, K, M, and channel realization, the average input-output mutual information of the symbol-level interleaved circular array setup is given by

$$E\left\{I\left(\boldsymbol{x}_1^M;\boldsymbol{y}^{CS}{}_1^M|\boldsymbol{S}_1^M,\mathcal{H}\right)\right\}=E\left\{\log\ \det\left(\boldsymbol{I}_N+\bar{P}\boldsymbol{S}^{CS}\boldsymbol{S}^{CS\dagger}\right)\right\}\quad , \tag{8-2}$$

where the channel transfer matrix $\boldsymbol{S}^{CS}$ is defined in (8-1), and the expectation is taken over all channel fades (denoted by $\mathcal{H}$), and over all spreading sequences. The notation $\boldsymbol{a}_1^M$ is used to designate the set of vectors $\boldsymbol{a_1},\ldots,\boldsymbol{a}_M$. Applying the Jensen inequality to (8-2) yields

$$E\left\{I\left(\boldsymbol{x}_1^M;\boldsymbol{y}^{CS}{}_1^M|\boldsymbol{S}_1^M,\mathcal{H}_{\mathcal{R}}\right)\right\}\leq E_{S_1^M}\left\{\log\ \det\left(\boldsymbol{I}_N+\bar{P}E_{\mathcal{H}}\{\boldsymbol{S}^{CS}\boldsymbol{S}^{CS\dagger}\}\right)\right\}\quad , \tag{8-3}$$

where the inner expectation is taken over all channel fades, and the outer expectation is taken over all spreading sequences. Due to the statistical independency of the fading matrices $\{\boldsymbol{H}_{n,m}\}$, all non-diagonal product blocks of $E_{\mathcal{H}}\{\boldsymbol{S}^{CS}\boldsymbol{S}^{CS\dagger}\}$ vanish in the expectation, and the latter expression becomes a block-diagonal matrix defined by

$$E_{\mathcal{H}}\{\boldsymbol{S}^{CS}\boldsymbol{S}^{CS\dagger}\}=\mathrm{diag}\left(\left\{\boldsymbol{S}_i\boldsymbol{S}_i^{\dagger}+\alpha^2\left(\boldsymbol{S}_{i^-}\boldsymbol{S}_{i^-}^{\dagger}+\boldsymbol{S}_{i^+}\boldsymbol{S}_{i^+}^{\dagger}\right)\right\}_{i=1}^{M}\right), \tag{8-4}$$

where

$$i^+=((M+i)\mod M)+1,$$

and

$$i^-=((M+i-2)\mod M)+1\ .$$

Hence, (8-3) boils down to

$$E\left\{I\left(\boldsymbol{x}_1^M;\boldsymbol{y}^{CS^M}_1|\boldsymbol{S}_1^M,\mathcal{H}\right)\right\}$$
$$\leq E_{S_1^M}\left\{\log\prod_{i=1}^{M}\det\left(\boldsymbol{I}_N+\bar{P}\left(\boldsymbol{S}_i\boldsymbol{S}_i^{\dagger}+\alpha^2\left(\boldsymbol{S}_{i^-}\boldsymbol{S}_{i^-}^{\dagger}+\boldsymbol{S}_{i^+}\boldsymbol{S}_{i^+}^{\dagger}\right)\right)\right)\right\}$$
$$= M\ E_{S_1^3}\left\{\log\ \det\left(\boldsymbol{I}_N+\bar{P}\tilde{\boldsymbol{S}}\tilde{\boldsymbol{S}}^{\dagger}\right)\right\}\quad , \quad (8\text{-}5)$$

where the last equality is due to the symmetrical nature of the circular array setup, and

$$\tilde{\boldsymbol{S}}\triangleq(\alpha\boldsymbol{S}_1\quad\boldsymbol{S}_2\quad\alpha\boldsymbol{S}_3)\quad . \quad (8\text{-}6)$$

Finally, using (8-5), the per-cell spectral efficiency of the optimum joint multiple cell-site receiver in this setup is upper bounded by

$$C^{CS}_{M\ \mathrm{opt}}\leq\lim_{\substack{N,K\to\infty\\ \frac{K}{N}\to\beta}}\frac{1}{N}E_{S_1^3}\left\{\log\ \det\left(\boldsymbol{I}_N+\bar{P}\tilde{\boldsymbol{S}}\tilde{\boldsymbol{S}}^{\dagger}\right)\right\}\quad . \quad (8\text{-}7)$$

Careful inspection of the above expression reveals that the RHS of the inequality is in fact equal to the spectral efficiency of the optimum receiver in a non-fading *single isolated cell* setup, accommodating $3K$ users. The $3K$ users are received at non-equal powers, with K users received at power $\bar{P}$, while the remaining $2K$ users are received at power $\alpha^2\bar{P}$. This setup, which is treated in [14], may be also interpreted as the extended cluster portion of the optimum spectral efficiency in the infinite linear array setup analyzed in Section 5, for the particular case of $M=1$ (see (5-7)). This spectral efficiency is given by

$$C_{3K\,\mathrm{opt}}=\beta\left[2\log(1+\alpha^2\eta\bar{P})+\log(1+\eta\bar{P})\right]+\log\frac{1}{\eta}+(\eta-1)\log e\quad , \quad (8\text{-}8)$$

where η is the unique solution to the following implicit equation

$$\eta+\beta\bar{P}\left[\frac{2\alpha^2\eta}{1+\alpha^2\eta\bar{P}}+\frac{\eta}{1+\eta\bar{P}}\right]=1\quad . \quad (8\text{-}9)$$

Simple numerical analysis shows that for any finite value of the cell load β, this upper bound surpasses the curve of the optimum receiver spectral efficiency obtained in the chip-

level interleaved circular array setup (6-9). However, as $\beta \to \infty$ (which is the optimum choice in terms of spectral efficiency in a single-cell setting), it is easily verified that

$$C_{3K_{\text{opt}}} = \log\left(1 + \beta(1+2\alpha^2)\bar{P}\right) + o(\beta^{-1}) \ . \tag{8-10}$$

But (8-10) is in fact identical to (6-15), designating the limiting spectral efficiency of the optimum receiver in the chip-interleaved setup as $\beta \to \infty$. Thus, we have established that as $\beta \to \infty$, the optimum spectral efficiency with chip-level interleaving coincides with the upper bound to the corresponding spectral efficiency in the symbol-interleaved setting.

8.2.2 Information Theoretic Bound

For every channel realization and any N, M and K, the conditional channel input-output mutual information of the symbol-level interleaved circular array setup (see (4-1) and (8-1)) satisfies the following relations

$$\begin{aligned} I\left(\boldsymbol{x}_1^M; \boldsymbol{y}^{CS}{}_1^M | \boldsymbol{S}_1^M, \mathcal{H}\right) &= h\left(\boldsymbol{y}^{CS}{}_1^M | \boldsymbol{S}_1^M, \mathcal{H}\right) - h\left(\boldsymbol{y}^{CS}{}_1^M | \boldsymbol{x}_1^M, \boldsymbol{S}_1^M, \mathcal{H}\right) \\ &= h\left(\boldsymbol{y}^{CS}{}_1^M | \boldsymbol{S}_1^M, \mathcal{H}\right) - h\left(\boldsymbol{n}_1^M\right) \\ &\overset{(a)}{\leq} \sum_{m=1}^{M} \left(h\left(\boldsymbol{y}^{CS}{}_m | \boldsymbol{S}_1^M, \mathcal{H}\right) - h\left(\boldsymbol{n}_m\right)\right) \\ &\overset{(b)}{=} M\left(h\left(\boldsymbol{y}^{CS}{}_2 | \boldsymbol{S}_1^M, \mathcal{H}\right) - h\left(\boldsymbol{n}_2\right)\right) \\ &= M\ I\left(\boldsymbol{x}_1^3; \boldsymbol{y}^{CS}{}_2 | \boldsymbol{S}_1^M, \mathcal{H}\right) \\ &= M\ \log\ \det\left(\boldsymbol{I}_N + \bar{P}\check{\boldsymbol{S}}\check{\boldsymbol{S}}^{\dagger}\right) \quad . \end{aligned} \tag{8-11}$$

In (8-11), (a) follows from the fact that $h(x,y) \leq h(x) + h(y)$ for any x,y arbitrary r.v's, (b) follows from the symmetrical nature of the circular array setup, and

$$\check{\boldsymbol{S}} \triangleq \left(\alpha \boldsymbol{S}_1 \boldsymbol{H}_{2,1} \quad \boldsymbol{S}_2 \boldsymbol{H}_{2,2} \quad \alpha \boldsymbol{S}_3 \boldsymbol{H}_{2,3}\right) \quad . \tag{8-12}$$

Hence, the per-cell spectral efficiency of the optimum joint multiple-cell-site receiver in this setup is upper bounded by

$$C^{CS}_{M\ \mathrm{opt}} \leq \lim_{\substack{N,K\to\infty \\ \frac{K}{N}\to\beta}} \frac{1}{N} E\left\{\log\ \det\left(\boldsymbol{I}_N + \bar{P}\check{\boldsymbol{S}}\check{\boldsymbol{S}}^{\dagger}\right)\right\} \quad , \tag{8-13}$$

where the expectation is taken over the spreading sequences and the relevant channel fades. As was the case with the Jensen bound considered in the previous subsection, careful inspection of (8-13) reveals that the RHS of the inequality equals the spectral efficiency achieved by an optimum receiver employed in a single isolated cell accommodating $3K$ users. The $3K$ users, operating in a flat-fading environment, use unequal transmit powers, with K users transmitting at power $\bar{P}$, while the remaining $2K$ users are transmitting at power $\alpha^2\bar{P}$. This setup, which is treated in [15] may also be interpreted as the extended cluster portion of the optimum spectral efficiency in the infinite linear array setup analyzed in Section 5, for the particular case of $M = 1$ (see (5-7)), in an analogous manner to Subsection 8.2.1. This spectral efficiency is given for the particular case of Rayleigh fading by

$$C^{F}_{3K_{\mathrm{opt}}} = \beta \log e \left[e^{\frac{1}{\bar{P}\eta}} E_1\left(\frac{1}{\bar{P}\eta}\right) + 2e^{\frac{1}{\alpha^2\bar{P}\eta}} E_1\left(\frac{1}{\alpha^2\bar{P}\eta}\right)\right] - \log\eta - \log e(1-\eta) \quad , \tag{8-14}$$

where $E_1(x) \triangleq \int_x^{\infty} \frac{e^{-t}}{t} dt,\ (t > 0)$ is the exponential integral, and η is the unique solution to the following implicit equation

$$\eta + \beta\bar{P}\left[3 - \frac{1}{\bar{P}\eta}\ e^{\frac{1}{\bar{P}\eta}} E_1\left(\frac{1}{\bar{P}\eta}\right) - \frac{2}{\alpha^2\bar{P}\eta}\ e^{\frac{1}{\alpha^2\bar{P}\eta}} E_1\left(\frac{1}{\alpha^2\bar{P}\eta}\right)\right] = 1 \quad . \tag{8-15}$$

Numerical analysis shows that for any finite value of the cell load β, this information theoretic upper bound also surpasses the curve of the spectral efficiency of the optimum receiver in a chip-level interleaved circular array setup (6-9). The current bound is however tighter than the previously considered Jensen bound, since non-homogeneous fading degrades the the spectral efficiency [6] [15]. On the other hand, when the cell load β is high, it is easily verified that

$$C^{F}_{3K_{\mathrm{opt}}} = \log\left(1 + \beta(1+2\alpha^2)\bar{P}\right) + o(\beta^{-1}) \quad , \tag{8-16}$$

which is again identical to (6-15). The same arguments used in Subsection 8.2.1 can therefore be applied to conclude the spectral efficiency with chip-level interleaving upper bounds the spectral efficiency with symbol-level interleaving in the high cell load region.

8.3 The Low-SNR Regime

8.3.1 Symbol-Level Interleaved Circular Array Setup

Consider the symbol-level interleaved circular array setup defined in Section 8.1. According to Theorem 8 of [17], the required $\frac{E_b^t}{N_0}$ for reliable communication is

$$\frac{E_b^t}{N_0}^{CS}_{\min} = \frac{KM \log_e 2}{E\left[\text{trace}\left\{\boldsymbol{S}^{CS\dagger}\boldsymbol{S}^{CS}\right\}\right]} \quad . \tag{8-17}$$

The denominator of (8-17) equals the expected *Frobenius* norm squared of the channel transfer matrix $\boldsymbol{S}^{CS}$ [17]

$$E\left[\text{trace}\left\{\boldsymbol{S}^{CS\dagger}\boldsymbol{S}^{CS}\right\}\right] = \sum_{i=1}^{MN}\sum_{j=1}^{MK} E\left[|\left(\boldsymbol{S}^{CS}\right)_{i,j}|^2\right] \quad , \tag{8-18}$$

and with the special structure of the $\boldsymbol{S}^{CS}$, as defined by (8-1), it is easy to verify that

$$\frac{E_b^t}{N_0}^{CS}_{\min} = \frac{\log_e 2}{m_2(1+2\alpha^2)} \quad , \tag{8-19}$$

where m_2 is the second power moment of an individual fading coefficient.

Turning to the low-SNR spectral efficiency slope of the optimum receiver, then according to Theorem 13 in [17] the low-SNR slope in the current setting is given by

$$S_0^{CS}{}_{\text{opt}} = \frac{2}{MN}\frac{\left(E\left[\text{trace}\left\{\boldsymbol{S}^{CS\dagger}\boldsymbol{S}^{CS}\right\}\right]\right)^2}{\left(E\left[\text{trace}\left\{\left(\boldsymbol{S}^{CS\dagger}\boldsymbol{S}^{CS}\right)^2\right\}\right]\right)} \quad . \tag{8-20}$$

Again, using the Frobenius norm equality of (8-18) for the product matrix $\left(\boldsymbol{S}^{CS\dagger}\boldsymbol{S}^{CS}\right)$, and the special structure of channel transfer matrix $\boldsymbol{S}^{CS}$, an explicit expression for the

low-SNR slope is obtained

$$S_{0\ \text{opt}}^{CS} = \frac{2\beta}{1+\beta}\left[1+\frac{(\mathcal{K}-1)(1+2\alpha^4)}{(1+\beta)(1+2\alpha^2)^2}\right]^{-1} \quad , \tag{8-21}$$

where $\mathcal{K}$ is the kurtosis of an individual fading coefficient (the kurtosis for a random variable a is defined as $\mathcal{K} = E[|a|^4]/(E[|a|^2])^2$). The slope of (8-21) may also be expressed as

$$S_{0\ \text{opt}}^{CS} = \frac{2\beta}{\mathcal{K}+\beta}\left[1-\frac{2(\mathcal{K}-1)\alpha^2(2+\alpha^2)}{(\mathcal{K}+\beta)(1+2\alpha^2)^2}\right]^{-1} \quad . \tag{8-22}$$

In the particular case of $\alpha = 0$, the above expression boils down, as expected, to the low-SNR slope of the optimum receiver in the single isolated cell setting $2\beta/(\mathcal{K}+\beta)$ [6]. The derivation of the above results is given in more details in App. C.

8.3.2 Non-Faded Circular Array Setup

Consider the symbol-level interleaver circular array setup defined in 8.1 in the absence of fading. In this setting one should take $\boldsymbol{H}_{i,j} = \boldsymbol{I}_K$ in (8-1), where $\boldsymbol{I}_K$ is a $K \times K$ identity matrix, and the resulting channel transfer matrix shall be denoted henceforth as $\boldsymbol{S}^{CNF}$. Using similar arguments to those of section 8.3.1, the minimum required $\frac{E_b^t}{N_0}$ for reliable communication is given by

$$\frac{E_b^t}{N_0}_{\min}^{CNF} = \frac{\log_e 2}{(1+2\alpha^2)} \quad , \tag{8-23}$$

while the low-SNR spectral efficiency slope of the optimum receiver is given by

$$S_{0\ \text{opt}}^{CNF} = \frac{2\beta}{1+\beta}\left[1+\frac{2\beta\alpha^2(4+\alpha^2)}{(1+\beta)(1+2\alpha^2)^2}\right]^{-1} \quad . \tag{8-24}$$

As was the case in Subsection 8.3.1, for the particular of $\alpha = 0$ the above slope coincides with the corresponding slope of the single-cell setting $2\beta/(1+\beta)$ [6]. See App. D for more details on the derivation.

8.3.3 Comparison

In this subsection the symbol-level interleaved, chip-level interleaved and non-fading circular array setups are compared. The comparison is performed in terms of the spectral

efficiency of the optimum receiver in the low-SNR regime.

Proposition 8.1 *The following statements hold with respect to the spectral efficiency of the optimum receiver in the low-SNR regime:*

(1). In the presence of fading, a chip-level interleaver is beneficial over a symbol-level interleaver.

(2). The presence of homogenous fading (chip-level interleaver) is beneficial over a no fading.

(3). Rayleigh flat-fading (symbol-level interleaver) is beneficial over no-fading in a certain range of the interference factor α, for $\beta > (\sqrt{33}-1)/16 \simeq 0.29$.

Proof: Assuming that the second power moment of an individual fading coefficient $m_2 = 1$, both fading setups require the same $\frac{E_b^t}{N_0}_{\min}$ to enable reliable communication (see (6-13) and (8-19) for the chip-level interleaved and symbol-level interleaved $\frac{E_b^t}{N_0}_{\min}$, respectively). Now, since $\mathcal{K} \geq 1$ for any arbitrary random variable, the expression in brackets in (8-21) is larger than 1, and recalling that the low-SNR spectral efficiency slope with a chip-level interleaver is $2\beta/(1+\beta)$, the first statement is proved.

The second statement is easily proved by noting that the expression in brackets of (8-24) is larger than 1 (for $\alpha > 0$).

A search for the conditions in which the ratio of the low-SNR slopes in the symbol-level interleaved setup (8-21) and in the non-faded setup (8-24) is greater than unity, yields after some algebra the following quadratic inequality (in α^2)

$$(\mathcal{K}-1) - 8\beta\alpha^2 + 2(\mathcal{K}-1-\beta)\alpha^4 < 0 \quad . \tag{8-25}$$

Focusing on Rayleigh fading ($\mathcal{K}=2$) reduces (8-25) to

$$1 - 8\beta\alpha^2 + 2(1-\beta)\alpha^4 < 0 \quad . \tag{8-26}$$

Investigation of this parametric quadratic inequality yields that for $\beta < (\sqrt{33}-1)/16 \simeq 0.296$ there is no solution to (8-26), and for this range of β values fading in not beneficial. On the other hand, if the cell load lies in the range $(\sqrt{33}-1)/16 \leq \beta < 3/10$, fading turn

out to be beneficial for an interval of the inter-cell interference factor $\alpha \in [\alpha_l, \alpha_h)$ where

$$\alpha_l = \sqrt{\frac{8\beta - \sqrt{64\beta^2 + 8\beta - 8}}{4(1-\beta)}} \quad ; \quad \alpha_h = \sqrt{\frac{8\beta + \sqrt{64\beta^2 + 8\beta - 8}}{4(1-\beta)}} \quad . \tag{8-27}$$

In addition, for $\beta \geq 3/10$ fading is beneficial for $\alpha \in [\alpha_l, 1]$, where α_l is given by (8-27). ■

It is also worth mentioning that α_l reduces to zero as the β increases (the expression for α_l is continuous at $\beta = 1$). This coincides with the results of [13], stating that when the number of users per cell goes to infinity, and all bandwidth is devoted to coding, fading is beneficial for all $\alpha \in [0, 1]$.

8.4 Multi-Antenna Model

A multi-antenna setup based on the setup presented and analyzed in [10] and [6] is analyzed. In this multi-antenna setup, a chip-level interleaver is employed. Each of the spreading chips of each user are affected by i.i.d fading coefficients at each receive antenna (independence across chips and antennas is assumed). The notation $(\cdot)^{MA}$ shall be used to denote quantities related to the chip-level interleaver multi-antenna setup. In this context, the received signal vector is given by

$$\boldsymbol{y}^{MA}_{[LN\times 1]} = \begin{pmatrix} \boldsymbol{S}_{[N\times\mathcal{K}]} \circ \boldsymbol{H}_{1[N\times\mathcal{K}]} \\ \cdots \\ \boldsymbol{S}_{[N\times\mathcal{K}]} \circ \boldsymbol{H}_{L[N\times\mathcal{K}]} \end{pmatrix} \boldsymbol{x}_{[K\times 1]} + \boldsymbol{n}_{[LN\times 1]} \quad , \tag{8-28}$$

where $\boldsymbol{H}_\ell$, $\ell = 1, \ldots, L$, is the matrix of i.i.d. zero-mean channel fading coefficients related to the ℓ-th receive antenna, satisfying

$$E\left\{|(\boldsymbol{H}_\ell)_{n,k}|^2\right\} = \frac{1}{L} \quad ; \quad \begin{matrix} 1 \leq n \leq N \\ 1 \leq k \leq K \end{matrix} \quad . \tag{8-29}$$

Applying similar arguments to those used for the multi-cell setups considered above, while assuming binary spreading sequences and circularly symmetric Gaussian fading coefficients, it is easily verified that the chip-interleaved multi-antenna model can be analyzed within the MIMO framework tools presented in [16] (see also Section 3). However, a more elegant

approach can be used via the following observation. A careful inspection of the system model of (8-28) shows that due to the resulting homogenous fading model, a single-cell interpretation can be employed in order to derive the spectral efficiency of the optimum and linear MMSE receiver. The chip-interleaved multi-antenna model is equivalent to a non-faded single isolated cell model with a *single* receive antenna, where the users employ random spreading sequences of length LN (with i.i.d. chips). In this case the spectral efficiency of the optimum and linear MMSE receivers are given by (6-10) and (6-9) respectively, while replacing the cell load β by β/L and $\bar{P}_{av}$ by $\bar{P}$. In addition, due to the fact that the spectral efficiency in bits/sec/Hz is normalized with respect to the *actual* length of the spreading sequences N, the expressions obtained for both receivers according to the single-cell interpretation should be scaled by the number of antennas L. Hence, for the linear MMSE receiver

$$C_{L\ \mathrm{ms}}^{MA} = \beta \log(1 + \eta_L^{MA} \bar{P}) \ , \tag{8-30}$$

and for the optimum receiver

$$C_{L\ \mathrm{opt}}^{MA} = C_{L\ \mathrm{ms}}^{MA} + L \log \frac{1}{\eta_L^{MA}} + L(\eta_L^{MA} - 1) \log e \ , \tag{8-31}$$

where η_L^{MA} is the unique solution to the following implicit equation

$$\eta_L^{MA} + \frac{\beta}{L} \frac{\eta_L^{MA} \bar{P}}{1 + \eta_L^{MA} \bar{P}} = 1 \quad . \tag{8-32}$$

The spectral efficiency of the optimum receiver can be more explicitly expressed as

$$C_{L\ \mathrm{opt}}^{MA} = \beta \log \left(1 + \bar{P} - \frac{1}{4} \mathcal{F}(\bar{P}, \frac{\beta}{L}) \right) + L \log \left(1 + \frac{\bar{P}\beta}{L} - \frac{1}{4} \mathcal{F}(\bar{P}, \frac{\beta}{L}) \right) - L \frac{\log e}{4\bar{P}} \mathcal{F}(\bar{P}, \frac{\beta}{L}) \ , \tag{8-33}$$

where $\mathcal{F}$ is defined in (6-12). With similar arguments it can be shown that the minimum energy per bit required for reliable communications satisfies $\frac{E_b^t}{N_0}_{\min}^{MA} = \frac{E_b^r}{N_0}_{\min}^{MA} = \log_e 2$, the

high-SNR spectral efficiency slopes of the receivers are given by

$$S_{\infty\ \mathrm{ms}}^{MA} = \begin{cases} \beta\ , & \beta < L \\ L/2\ , & \beta = L \\ 0\ , & \beta > L \end{cases} \quad , \tag{8-34}$$
$$S_{\infty\ \mathrm{opt}}^{MA} = \min(\beta, L) \quad ,$$

and the low-SNR spectral efficiency slopes are

$$\begin{aligned} S_{0\ \mathrm{ms}}^{MA} &= \frac{2\beta L}{L+2\beta}\ , \\ S_{0\ \mathrm{opt}}^{MA} &= \frac{2\beta L}{L+\beta} \quad . \end{aligned} \tag{8-35}$$

In addition, in the high cell load region, it is easily verified that

$$\eta_L^{MA} = \frac{1}{1+\frac{\beta}{L}\bar{P}} + o(\beta^{-1}) \quad , \tag{8-36}$$

and the spectral efficiencies reduce to

$$\begin{aligned} C_{L\ \mathrm{ms}}^{MA} &= L(1-\eta_L^{MA})\log e + o(\beta^{-1}) \\ C_{L\ \mathrm{opt}}^{MA} &= (L-1)(1-\eta_L^{MA})\log e + L\log\frac{1}{\eta_L^{MA}} + o(\beta^{-1}) \quad . \end{aligned} \tag{8-37}$$

For the sake of comparison, the multi-antenna setup presented and analyzed in [10] and [6], is also considered. In this setup, a symbol-level interleaver is employed resulting in a non-homogeneous fading process as described in the beginning of this section. The notation $(\cdot)^{MAS}$ shall be used to denote quantities related to the symbol-level interleaver multi-antenna setup. In this context, the received vector at the multi-antenna receiver is given by

$$\boldsymbol{y}_{[LN\times 1]}^{MAS} = \begin{pmatrix} \boldsymbol{S}_{[N\times\mathcal{K}]}\boldsymbol{H}_{1[K\times\mathcal{K}]} \\ \cdots \\ \boldsymbol{S}_{[N\times\mathcal{K}]}\boldsymbol{H}_{L[K\times\mathcal{K}]} \end{pmatrix} \boldsymbol{x}_{[K\times 1]} + \boldsymbol{n}_{[LN\times 1]} \quad , \tag{8-38}$$

where $\boldsymbol{H}_\ell \triangleq \mathrm{diag}\,(A_{k,\ell})_{k=1}^{K}$, $\ell = 1, \ldots, L$, is the diagonal matrix of channel fading coefficients corresponding to the ℓ-th receive antenna. The fading coefficients are assumed to

be i.i.d., and satisfy

$$E\left\{|A_{k,\ell}|^2\right\} = \frac{1}{L} \quad ; \quad \begin{array}{c} 1 \le k \le K \\ 1 \le \ell \le L \end{array} \quad . \tag{8-39}$$

The spectral efficiencies of the linear MMSE and optimum receiver in this setup are derived in [6], and given by

$$\begin{aligned} C_L^{MAS}{}_{\text{ms}} &= \beta E\left\{\log(1+\eta_L^{MAS}\bar{P}|\bar{A}|^2)\right\} \\ C_L^{MAS}{}_{\text{opt}} &= C_L^{MAS}{}_{\text{ms}} + \log\frac{1}{\eta_L^{MAS}} + (\eta_L^{MAS}-1)\log e \quad , \end{aligned} \tag{8-40}$$

where η^{MAS} is the unique solution to the following implicit equation

$$\eta_L^{MAS} + \frac{\beta}{L} E\left\{\frac{\bar{P}|\bar{A}|^2\eta_L^{MAS}}{1+\bar{P}|\bar{A}|^2\eta_L^{MAS}}\right\} = 1 \quad . \tag{8-41}$$

The expectations in (8-40) and (8-41) are with respect to the distribution of

$$|\bar{A}|^2 = \sum_{\ell=1}^{L} |A_{1,\ell}|^2 \quad , \tag{8-42}$$

where $A_{1,\ell}$ is the fading coefficient associated with user 1 and the ℓ-th receive antenna (note that the fades are i.i.d. across users and antennas).

According to [6], the minimum energy per bit required for reliable communication $\frac{E_b^t}{N_0}{}_{\min}^{MAS} = \frac{E_b^r}{N_0}{}_{\min}^{MAS} = \log_e 2$, and the low-SNR spectral efficiencies slopes are given by

$$\begin{aligned} S_0^{MAS}{}_{\text{ms}} &= \frac{2\beta L}{L\mathcal{K}(|\bar{A}|)+2\beta} \\ S_0^{MAS}{}_{\text{opt}} &= \frac{2\beta L}{L\mathcal{K}(|\bar{A}|)+\beta+\beta\,(1-1/L)} \quad , \end{aligned} \tag{8-43}$$

where $\mathcal{K}(|\bar{A}|)$ is the kurtosis of $|\bar{A}|$. Since the kurtosis of an arbitrary random variable is greater than one, it is clear that the low-SNR slopes of the chip-level interleaver multi-antenna setup of (8-35), surpass the low-SNR slopes of the symbol-level interleaver multi-antenna setup of (8-43). The high-SNR spectral efficiency slopes are also derived in [6]

and given by

$$S_{\infty}^{MAS}{}_{\text{ms}} = \begin{cases} \beta \ , & \beta < L \\ L/2 \ , & \beta = L \\ 0 \ , & \beta > L \end{cases}$$
$$S_{\infty}^{MAS}{}_{\text{opt}} = \begin{cases} \beta \ , & \beta < L \\ (L+1)/2 \ , & \beta = L \\ 1 \ , & \beta > L \ . \end{cases} \tag{8-44}$$

In the high-SNR regime, the spectral efficiency slopes of the linear MMSE receiver in both multi-antenna setups, as given by (8-34) and (8-44), coincide. Turning to the optimum receiver, the difference between the high-SNR slopes in the two setups is

$$\Delta S_{\infty_{\text{opt}}} = S_{\infty}^{MA}{}_{\text{opt}} - S_{\infty}^{MAS}{}_{\text{opt}} = \begin{cases} 0 \ , & \beta < L \\ (L-1)/2 \ , & \beta = L \\ L-1 & L \leq \beta \quad . \end{cases} \tag{8-45}$$

As can be observed, the slope in the chip-level interleaved setup is always higher or equal to the slope in the symbol-level interleaved setup.

The high cell load region of the symbol-level interleaved setup is also analyzed in [6], and it can be shown that

$$\eta_L^{MAS} = \frac{1}{1+\frac{\beta}{L}\bar{P}} + o(\beta^{-1}) \quad , \tag{8-46}$$

and the spectral efficiencies of the two receivers are given by

$$\begin{aligned} C_L^{MAS}{}_{\text{ms}} &= L(1-\eta_L^{MAS})\log e + o(\beta^{-1}) \\ C_L^{MAS}{}_{\text{opt}} &= (L-1)(1-\eta_L^{MAS})\log e + \log\frac{1}{\eta_L^{MAS}} + o(\beta^{-1}) \quad . \end{aligned} \tag{8-47}$$

Comparing (8-46) and (8-36), it is observed that $\eta_L^{MAS} = \eta_L^{MA}$. Hence, the spectral efficiency of the linear MMSE receiver in both setups, as given by (8-37) and (8-47), coincide. In contrast, the spectral efficiency of the optimum receiver in the chip-level interleaved setup is significantly higher than that of the corresponding receiver in the symbol-level interleaved

setup. Comparing (8-37) and (8-47), the spectral efficiency difference is given by

$$\Delta C_{L_{\text{opt}}} \underset{\beta\to\infty}{=} C_L^{MA}{}_{\text{opt}} - C_L^{MAS}{}_{\text{opt}} = (L-1)\log(1+\frac{\beta}{L}\bar{P}) + o(\beta^{-1}) \quad , \tag{8-48}$$

which is bounded for $L \gg 1$ by $\beta\bar{P}$ (note that $\beta\bar{P}$ is finite whenever the spectral efficiency and E_b/N_0 are finite, regardless of the value of β, as can be observed from (3-9)).

9 Concluding Remarks

This report examines the effect of joint multiple-cell-site processing on the performance of randomly spread DS-CDMA systems, for three variants of Wyner's infinite linear cell-array model [11]: 1) An isolated cluster of M cells; 2) An infinite linear cell-array divided into clusters of M-cells, which are seperately processed; 3) M cells arranged on a circle. Chip-level interleaver is used in order to form an uncorrelated Gaussian channel transfer matrix, which in the single-cell setup yields the *homogeneous* fading channel model [5]. The resulting model may be interpreted as a single-user MIMO channel analogous to the channel analyzed in [16]. Expressions for the spectral efficiencies of the optimum and linear MMSE joint multiple cell-site receivers in the three multi-cell settings were derived, as well as expressions for the low- and high-SNR spectral efficiency slopes, and the limiting spectral efficiency in the high cell load region. The results can be straightforwardly extended from the Wyner framework to include the case in which each cell-site receives the signals of more than just the two adjacent cells.

Analysis of the per-cell spectral efficiencies shows that the joint multiple-cell-site strategy *dramatically* enhances system performance for both receivers. Focusing on the infinite cell-array setup, this dramatic performance enhancement is demonstrated by showing that for $\alpha = 1/2$ the spectral efficiency attained with the joint 3-cell-site *linear* MMSE receiver, always surpasses the much more complex (!) *optimum* single-cell-site processor [15]. Considering the transmit $E_b/N_{0_{\min}}$, the joint multiple-cell-site processing scheme produces an energy gain of $\left[1+2\alpha^2\left(1-\frac{1}{M}\right)\right]$ as compared to single cell-site processing. The low-SNR spectral efficiency slopes of the two receivers coincide, as the cluster size M grows, with the corresponding slopes in the single-cell non-fading setup [6], and the optimality of increasing β without bound in the low SNR regime is established. However, beyond a critical

value of E_b/N_0 the optimum choice for β decreases from infinity and takes on finite values, approaching for the optimum receiver the value of $M/(M+2)$ in the high SNR regime. In fact, the linear MMSE receiver becomes *interference limited* for $\beta \to \infty$, where as the optimum receiver is not interference limited for $M \geq 3$. However, some amount of spreading is still beneficial for the optimum receiver for any finite value of the cluster size M. In the limiting setup in which *both* $M, \beta \to \infty$ the effect of random spreading is eliminated, and the spectral efficiency of the optimum receiver coincides with the corresponding result for the non-spread Rayleigh flat-fading Wyner model [13] (which always *surpasses* the one attained in the absence of fading [11]). This comes in contrast to single-cell-site processing, for which homogeneous fading has no effect on system performance [6] (as compared to a non-faded setup), and demonstrates the beneficial effect of fading when optimum joint multiple-cell-site processing is employed.

Comparison of the above results to the corresponding results in the isolated cluster setup, demonstrates the impact of inter-cluster interference on system performance. The spectral efficiencies in the isolated cluster setting are shown to approach much faster with the cluster size M (as compared to the corresponding results in the infinite cell-array setting) the high-M spectral efficiency limit, as represented by the results of the circular-array model. In the latter model, the per-cell spectral efficiencies of the two receivers coincide with the corresponding spectral efficiencies in a *single-cell* non-fading setup [6], but with received SNR *increased* by a factor of $(1+2\alpha^2)$.

The circular-array setup is also used to investigate the impact of chip-level interleaving on system performance. Focusing on the spectral efficiency of the optimum receiver, it is shown that for $\beta \to \infty$ (which is the optimum choice in terms of spectral efficiency in the circular setting) the spectral efficiency with chip-level interleaving coincides with upper bounds on the spectral efficiency attained with symbol-level interleaving. Considering the low-SNR regime it is shown that in the presence of fading chip-level interleaving is beneficial over symbol-level interleaving. Comparison to the corresponding low-SNR regime in the absence of fading shows that the homogeneous fading model resulting from chip-level interleaving is beneficial. In addition, it is shown that the low-SNR spectral efficiency with Rayleigh flat-fading and a symbol-level interleaver surpasses the corresponding spectral efficiency in the absence of fading for a certain range of the interference factor α and β. This comes in contrast to the effect of fading in the case of single-cell-site processing, where non-

homogeneous fading always degrades system performance. To complete the investigation, a single-cell multiple-receive-antenna model is also considered. It is shown that in the low SNR regime, the spectral efficiencies with chip-level interleaving always surpass the ones with symbol-level interleaving for both the linear MMSE and optimum receiver. In the high-SNR regime, the spectral efficiency slope of the linear MMSE receiver remains the same with both interleaving schemes. In contrast, for the optimum receiver the slope is higher with chip-level interleaving when the cell-load is higher than the number of receive antennas. For $\beta \to \infty$ the spectral efficiencies of the linear MMSE receiver coincide for both interleaving schemes, while for the optimum receiver the spectral efficiency with chip-level interleaving is always higher than the one attained with symbol-level interleaving. In view of the above results, it is conjectured that with optimum processing chip-level interleaving is beneficial in terms of spectral efficiency in general.

A Proof of Theorem 6.1

Let $\{\boldsymbol{y}_1^{IC},\ldots,\boldsymbol{y}_M^{IC}\}$ and $\{\boldsymbol{y}_1^{C},\ldots,\boldsymbol{y}_M^{C}\}$ denote the sets of received signal vectors in each of the M cell-sites in the setups of M-cells isolated cluster, and a circular array of M cells, respectively. Let $\{\boldsymbol{x}_1,\ldots,\boldsymbol{x}_M\}$ denote the set of input signal vectors from users in the corresponding cells. Recall that the statistical properties of the input signals, as defined in Section 2, are independent of the particular arrangement of cell-sites (and no cooperation between different users is assumed). With the above notation, the following set of mutual information relations holds *for any channel realization and any value of K, N, and $M \geq 3$*:

$$\begin{aligned}
&I_{(M)}(\boldsymbol{x}_1,\ldots,\boldsymbol{x}_M\,;\,\boldsymbol{y}_1^{C},\ldots,\boldsymbol{y}_M^{C}) \\
&\overset{(a)}{\geq} I_{(M)}(\boldsymbol{x}_1,\ldots,\boldsymbol{x}_M\,;\,\boldsymbol{y}_1^{C},\ldots,\boldsymbol{y}_M^{C}\,|\,\boldsymbol{x}_M=\boldsymbol{0}) \\
&= I_{(M)}(\boldsymbol{x}_1,\ldots,\boldsymbol{x}_{M-1}\,;\,\boldsymbol{y}_1^{C},\ldots,\boldsymbol{y}_M^{C}\,|\,\boldsymbol{x}_M=\boldsymbol{0}) \\
&\overset{(b)}{\geq} I_{(M)}(\boldsymbol{x}_1,\ldots,\boldsymbol{x}_{M-1}\,;\,\boldsymbol{y}_1^{C},\ldots,\boldsymbol{y}_{M-1}^{C}\,|\,\boldsymbol{x}_M=\boldsymbol{0}) \\
&\overset{(c)}{=} I_{(M-1)}(\boldsymbol{x}_1,\ldots,\boldsymbol{x}_{M-1}\,;\,\boldsymbol{y}_1^{IC},\ldots,\boldsymbol{y}_{M-1}^{IC}) \quad ,
\end{aligned} \tag{A-1}$$

where the subscript $(\cdot)_{(M)}$ denotes that the mutual information relates to a setup of M cells (arranged either in a linear array or a circular array). Inequality (a) follows the fact that conditioning reduces entropy (and that the channel is an additive noise channel). Inequality (b) follows from the fact that information can only be lost if the (overall) received signal vector is truncated. Finally, equality (c) holds because with the preceding input constraints and the output truncation, a circular array of M cells is equivalent to a *linear array* of $M-1$ isolated cells. But

$$C_{\text{opt}}^{C} = \frac{1}{M}\lim_{\substack{N,K\to\infty \\ \frac{K}{N}\to\beta}} \frac{1}{N} E\left\{I_{(M)}(\boldsymbol{x}_1,\ldots,\boldsymbol{x}_M\,;\,\boldsymbol{y}_1^{C},\ldots,\boldsymbol{y}_M^{C})\right\} \quad , \tag{A-2}$$

and

$$C_{M\,\text{opt}}^{IC} = \frac{1}{M}\lim_{\substack{N,K\to\infty \\ \frac{K}{N}\to\beta}} \frac{1}{N} E\left\{I_{(M)}(\boldsymbol{x}_1,\ldots,\boldsymbol{x}_M\,;\,\boldsymbol{y}_1^{IC},\ldots,\boldsymbol{y}_M^{IC})\right\} \quad . \tag{A-3}$$

Hence, it follows that

$$MC_{\text{opt}}^{C} \geq (M-1)C_{(M-1)_{\text{opt}}}^{IC} \ , \tag{A-4}$$

or

$$C^{C}_{\text{opt}} \geq \left(1 - \frac{1}{M}\right) C^{IC}_{(M-1)_{\text{opt}}} \quad . \tag{A-5}$$

To upper bound the spectral efficiency of the optimum receiver in the circular setup we use the following set of mutual information relations:

$$\begin{aligned}
&I_{(M)}(\boldsymbol{x}_1, \ldots, \boldsymbol{x}_M \,;\, \boldsymbol{y}^C_1, \ldots, \boldsymbol{y}^C_M) \\
&\quad = I_{(M)}(\boldsymbol{x}_1, \boldsymbol{x}_M \,;\, \boldsymbol{y}^C_1, \ldots, \boldsymbol{y}^C_M) + I_{(M)}(\boldsymbol{x}_2, \ldots, \boldsymbol{x}_{M-1} \,;\, \boldsymbol{y}^C_1, \ldots, \boldsymbol{y}^C_M \,|\, \boldsymbol{x}_1, \boldsymbol{x}_M) \\
&\quad \overset{(a)}{=} I_{(M)}(\boldsymbol{x}_1, \boldsymbol{x}_M \,;\, \boldsymbol{y}^C_1, \ldots, \boldsymbol{y}^C_M) + I_{(M)}(\boldsymbol{x}_2, \ldots, \boldsymbol{x}_{M-1} \,;\, \boldsymbol{y}^{IC}_1, \ldots, \boldsymbol{y}^{IC}_M \,|\, \boldsymbol{x}_1, \boldsymbol{x}_M) \\
&\quad = I_{(M)}(\boldsymbol{x}_1, \boldsymbol{x}_M \,;\, \boldsymbol{y}^C_1, \ldots, \boldsymbol{y}^C_M) - I_{(M)}(\boldsymbol{x}_1, \boldsymbol{x}_M \,;\, \boldsymbol{y}^{IC}_1, \ldots, \boldsymbol{y}^{IC}_M) \\
&\qquad + I_{(M)}(\boldsymbol{x}_1, \boldsymbol{x}_M \,;\, \boldsymbol{y}^{IC}_1, \ldots, \boldsymbol{y}^{IC}_M) + I_{(M)}(\boldsymbol{x}_2, \ldots, \boldsymbol{x}_{M-1} \,;\, \boldsymbol{y}^{IC}_1, \ldots, \boldsymbol{y}^{IC}_M \,|\, \boldsymbol{x}_1, \boldsymbol{x}_M) \\
&\quad = I_{(M)}(\boldsymbol{x}_1, \boldsymbol{x}_M \,;\, \boldsymbol{y}^C_1, \ldots, \boldsymbol{y}^C_M) - I_{(M)}(\boldsymbol{x}_1, \boldsymbol{x}_M \,;\, \boldsymbol{y}^{IC}_1, \ldots, \boldsymbol{y}^{IC}_M) \\
&\qquad + I_{(M)}(\boldsymbol{x}_1, \ldots, \boldsymbol{x}_M \,;\, \boldsymbol{y}^{IC}_1, \ldots, \boldsymbol{y}^{IC}_M) \\
&\quad \leq I_{(M)}(\boldsymbol{x}_1, \boldsymbol{x}_M \,;\, \boldsymbol{y}^C_1, \ldots, \boldsymbol{y}^C_M) + I_{(M)}(\boldsymbol{x}_1, \ldots, \boldsymbol{x}_M \,;\, \boldsymbol{y}^{IC}_1, \ldots, \boldsymbol{y}^{IC}_M) \quad .
\end{aligned} \tag{A-6}$$

Here, inequality (a) follows from the fact that given the inputs from cells 1 and M the mutual information in the second term is identical for both linear (isolated cluster) and circular setups. Now examining the first term in the RHS of the inequality of (A-6), we observe that

$$\begin{aligned}
I_{(M)}(\boldsymbol{x}_1, \boldsymbol{x}_M \,;\, \boldsymbol{y}^C_1, \ldots, \boldsymbol{y}^C_M) &\leq I_{(M)}(\boldsymbol{x}_1, \boldsymbol{x}_M \,;\, \boldsymbol{y}^C_1, \ldots, \boldsymbol{y}^C_M \,|\, \boldsymbol{x}_2 = \cdots = \boldsymbol{x}_{M-1} = \boldsymbol{0}) \\
&= I_{(M)}(\boldsymbol{x}_1, \boldsymbol{x}_M \,;\, \boldsymbol{y}^C_1, \boldsymbol{y}^C_2, \boldsymbol{y}^C_{M-1}, \boldsymbol{y}^C_M \,|\, \boldsymbol{x}_2 = \boldsymbol{x}_{M-1} = \boldsymbol{0}) \\
&\triangleq \mathcal{K}_1 \quad ,
\end{aligned} \tag{A-7}$$

where $\mathcal{K}_1$ is fixed and independent of M ($M \geq 3$) for any fixed $\bar{P}$, α and β. The inequality in (A-7) follows from the fact the the mutual information in the LHS of the inequality designates the achievable sum-rate when decoding only the users of cells 1 and M, while taking into account the structure of the interference generated by the users operating in all other cells within the circular array, and therefore eliminating all other-cell interference can only increase the achievable rate. The equality in (A-7) straightforwardly follows from the fact that without any transmissions in cells 2 to $M-1$, the signals received in cell-sites 3 to $M-2$ include only AWGN and therefore do not contribute to the mutual information

in the LHS of the equality. Combining (A-7) and (A-6) with (A-2) and (A-3), the spectral efficiency of the optimum receiver for the circular array can be upper bounded by

$$C^{C}_{\text{opt}} \leq C^{IC}_{M\,\text{opt}} + \frac{\mathcal{K}_1}{M} \quad . \tag{A-8}$$

Finally, from (A-5) and (A-8) it follows that

$$C^{C}_{\text{opt}} - \frac{\mathcal{K}_1}{M} \leq C^{IC}_{M\,\text{opt}} \leq \left(1 - \frac{1}{M+1}\right)^{-1} C^{C}_{\text{opt}} \quad , \tag{A-9}$$

and taking the limit as $M \to \infty$, while recalling that C^{C}_{opt} is independent of M for $M \geq 3$, it follows that

$$\lim_{M\to\infty} C_{M\,\text{opt}} = C^{C}_{\text{opt}} \quad . \tag{A-10}$$

Now in order to show that the same asymptotic result also holds for the infinite linear array setup of Section 5, recall first that according to (5-6)

$$C^{IA}_{M\,\text{opt}} = \mathcal{C}_M - \frac{2}{M}\mathcal{C}_I \quad . \tag{A-11}$$

Clearly, the term $\mathcal{C}_I$, as given by (5-21), is fixed for any fixed $\bar{P}$, α and β, and is independent of M. It therefore remains to investigate the behavior of $\mathcal{C}_M$ as M grows large. Clearly $\mathcal{C}_M$ is lower bounded by $C^{IC}_{M\,\text{opt}}$ in view of (A-3), (5-7) and the following mutual information relations

$$\begin{aligned} I\left(\boldsymbol{x}_0^{M+1}\,;\,\boldsymbol{y}^{IA}{}_1^{M}\right) &\geq I\left(\boldsymbol{x}_0^{M+1}\,;\,\boldsymbol{y}^{IA}{}_1^{M}\,|\,\boldsymbol{x}_0 = \boldsymbol{x}_{M+1} = \boldsymbol{0}\right) \\ &= I\left(\boldsymbol{x}_1^{M}\,;\,\boldsymbol{y}^{IA}{}_1^{M}\,|\,\boldsymbol{x}_0 = \boldsymbol{x}_{M+1} = \boldsymbol{0}\right) \\ &= I\left(\boldsymbol{x}_1^{M}\,;\,\boldsymbol{y}^{IC}{}_1^{M}\right) \quad . \end{aligned} \tag{A-12}$$

A simple upper bound to $\mathcal{C}_M$ can be derived by observing that (assuming an array of no more than $M+2$ active cells)

$$I\left(\boldsymbol{x}_0^{M+1}\,;\,\boldsymbol{y}^{IC}{}_0^{M+1}\right) \geq I\left(\boldsymbol{x}_0^{M+1}\,;\,\boldsymbol{y}^{IC}{}_1^{M}\right) = I\left(\boldsymbol{x}_0^{M+1}\,;\,\boldsymbol{y}^{IA}{}_1^{M}\right) \quad , \tag{A-13}$$

and hence (again following (A-3) and (5-7))

$$\mathcal{C}_M \leq (1 + \frac{2}{M})C^{IC}_{(M+2)_{\text{opt}}} \quad . \tag{A-14}$$

But from (A-10) it is seen that both upper and lower bound on $\mathcal{C}_M$ converge to the same limit C^C_{opt} as $M \to \infty$, which completes the proof of the Theorem, since the term $\frac{2}{M}\mathcal{C}_I$ in (5-6) vanishes with M. ■

B Proofs Related to the Infinite Array Setup

B.1 Minimum E_b/N_0

The minimum transmitted energy per bit required for reliable communication is expressed in [17] by

$$\frac{E_b^t}{N_{0\,\min}} \triangleq \frac{\beta}{\dot{C}_{\text{opt}}(0)} \quad , \tag{B-1}$$

where the derivative is with respect to the transmit SNR $\bar{P}$. Substituting (5-6) into (B-1) yields

$$\begin{aligned} \frac{E_b^{t\,IA}}{N_{0\,min}} &= \frac{\beta}{\dot{\mathcal{C}}_M(0) - \frac{2}{M}\dot{\mathcal{C}}_I(0)} \\ &= \frac{\beta}{\tilde{\beta}\left(\frac{E_b^{t\,M}}{N_{0\,\min}}\right)^{-1} - \frac{2}{M}\beta\left(\frac{E_b^{t\,I}}{N_{0\,\min}}\right)^{-1}} \quad , \end{aligned} \tag{B-2}$$

where $\frac{E_b^{t\,M}}{N_{0\,\min}}$ is the transmit $\frac{E_b}{N_{0\,\min}}$ of the extended cluster receiver that corresponds to $\mathcal{C}_M$ in (5-7), $\frac{E_b^{t\,I}}{N_{0\,\min}}$ is the transmit $\frac{E_b}{N_{0\,\min}}$ of the isolated single-cell setup that corresponds to $\mathcal{C}_I$ in (5-8), and $\tilde{\beta}$ is the system average cell load of the extended cluster as defined by (5-10). Using (3-10) and (5-12), we get

$$\frac{E_b^{t\,M}}{N_{0\,\min}} = \frac{\log_e 2}{(1+2\alpha^2)}\frac{M+2}{M} \quad , \tag{B-3}$$

and

$$\frac{E_b^{t\,I}}{N_{0\,\min}} = \frac{\log_e 2}{\alpha^2} \quad . \tag{B-4}$$

Substituting (B-3) and (B-4) into (B-2) finally yields (5-24).

B.2 Low-SNR Spectral Efficiency Slope

B.2.1 Optimum Receiver

The low-SNR spectral efficiency slope of the optimum receiver is expressed in [17] as

$$S_0 \triangleq \frac{2\left[\dot{C}(0)\right]^2}{-\ddot{C}(0)} \quad , \tag{B-5}$$

where the derivatives are with respect to the transmitted signal-to-noise ratio $\bar{P}$. Using (5-6), (B-1), (B-5) and some algebra we get for $M \geq 2$

$$S_{0_{\text{opt}}}^{IA} = \frac{\left(\frac{E_b^t}{N_0}^{IA}_{\min}\right)^{-2}\beta^2}{\frac{1}{S_{0_{\text{opt}}}^{M}}\left(\frac{E_b^t}{N_0}^{M}_{\min}\right)^{-2}\tilde{\beta}^2 - \frac{2}{M}\frac{1}{S_{0_{\text{opt}}}^{I}}\left(\frac{E_b^t}{N_0}^{I}_{\min}\right)^{-2}\beta^2} \quad , \tag{B-6}$$

where $(S_{0_{\text{opt}}}^{M}, \frac{E_b^t}{N_0}^{M}_{\min}, \tilde{\beta})$ and $(S_{0_{\text{opt}}}^{I}, \frac{E_b^t}{N_0}^{I}_{\min}, \beta)$ are the low-SNR spectral efficiency slope, the minimum transmitted energy per bit, and the system average cell load of the optimum receiver in the extended cluster, and in the isolated single cell, respectively.

In order to obtain $S_{0_{\text{opt}}}^{M}$ it is required to calculate the total normalized power injected by the j-th transmit antenna, and the normalized power collected by the i-th receive antenna of the equivalent MIMO model, as defined by (3-12) and (3-13). These are given for $M \geq 2$ by

$$P_T(j) = \begin{cases} \alpha^2 \frac{1}{g^{IA}} \ , & j = 0, M+1 \\ (1+\alpha^2)\frac{1}{g^{IA}} \ , & j = 1, M \\ (1+2\alpha^2)\frac{1}{g^{IA}} \ , & 2 \leq j \leq M-1 \end{cases} \quad , \tag{B-7}$$

and

$$P_R(i) = (1+2\alpha^2)\frac{\beta}{g^{IA}} \quad ; \quad 1 \leq i \leq M \quad , \tag{B-8}$$

respectively. Substituting (B-7) and (B-8) into (B-5), yields for $M \geq 2$

$$S_{0_{\text{opt}}}^{M} = \frac{2\beta}{1+\beta}\frac{\left(1+2\alpha^2\right)^2}{1+4\left(1-\frac{1}{(1+\beta)M}\right)\alpha^2+4\left(1-\frac{1}{(1+\beta)M}\right)\alpha^4} \quad . \tag{B-9}$$

To complete the derivation recall that the low-SNR slope of the optimum receiver in the isolated single-cell setup is given in [6] by

$$S_{0_{\text{opt}}}^{I} = \frac{2\beta}{1+\beta} \quad . \tag{B-10}$$

Now, substituting (B-9) and (B-10) into (B-6) finally yields (5-25).

B.2.2 Linear MMSE Receiver

In the low SNR regime ($\bar{P} \ll 1$), it is easy to verify that $\Gamma_M^{IA}(m)$, as defined by (5-16), is approximated well for $M \geq 2$ by

$$\begin{aligned} \beta\left(1+2\alpha^2\right)\Gamma_M^{IA}(m) &= \sum_{l=m-1}^{m+1} [\boldsymbol{\mathcal{P}}_M^{IA}]_{l,m}\left(1 - \sum_{k=l-1}^{l+1} [\boldsymbol{\mathcal{P}}_M^{IA}]_{l,k}\beta\bar{P}\right) + O(\bar{P}^2) \\ & m = 1,2,\ldots,M \quad , \end{aligned} \tag{B-11}$$

where out-of-range indices should be ignored. Using the special structure of the discrete-index asymptotic power profile of the infinite cell-array setup, $\boldsymbol{\mathcal{P}}_M^{IA}$, as defined by (5-15), it follows that (B-11) boils down to

$$\begin{aligned} \beta\left(1+2\alpha^2\right)\Gamma_M^{IA}(m) &= a_m - b_m\bar{P} + O(\bar{P}^2) \\ & m = 1,2,\ldots,M \quad , \end{aligned} \tag{B-12}$$

where

$$a_m = \begin{cases} 1+\alpha^2 \ , & m = 1, M \\ 1+2\alpha^2 \ , & 2 \leq m \leq M-1 \end{cases} \quad , \tag{B-13}$$

and

$$\begin{aligned} M = 2 \quad &: \quad b_1 = 1+2\alpha^2+2\alpha^4 \quad , \\ M = 3 \quad &: \quad b_1 = 1+2\alpha^2+2\alpha^4 \quad ; \quad b_2 = 1+4\alpha^2+3\alpha^4 \quad , \\ M \geq 4 \quad &: \quad b_m = \begin{cases} 1+2\alpha^2+2\alpha^4 \ , & m = 1, M \\ 1+4\alpha^2+3\alpha^4 \ , & m = 2, M-1 \\ 1+4\alpha^2+4\alpha^4 \ , & 3 \leq m \leq M-2 \ . \end{cases} \end{aligned} \tag{B-14}$$

In addition, it is easily verified that in the low-SNR regime, every summand in the expression for the spectral efficiency of the linear MMSE receiver (5-23) reduces to

$$\log\left(1+\Gamma_M^{IA}(m)(1+2\alpha^2)\beta\bar{P}\right)=\left(a_m\bar{P}-\frac{1}{2}\left(2b_m+a_m^2\right)\bar{P}^2\right)\log e+O(\bar{P}^3) \qquad m=1,2,\ldots,M \quad . \tag{B-15}$$

Now, substituting (B-15) in (5-23) it follows that the low-SNR spectral efficiency of the linear MMSE receiver is approximated by

$$\begin{aligned}
M=2 \;:\; & C_{M\,\mathrm{ms}}^{IA}(\bar{P})=\frac{\beta}{2}\left[2a_1\bar{P}-\frac{1}{2}\left(4b_1+2a_1^2\right)\bar{P}^2\right]\log e+O(\bar{P}^3) \quad , \\
M=3 \;:\; & C_{M\,\mathrm{ms}}^{IA}(\bar{P})=\frac{\beta}{3}\left[\left(2a_1+a_2\right)\bar{P}-\frac{1}{2}\left(4b_1+2b_2+2a_1^2+a_2^2\right)\bar{P}^2\right]\log e+O(\bar{P}^3) \quad , \\
M\geq 4 \;:\; & C_{M\,\mathrm{ms}}^{IA}(\bar{P})=\frac{\beta}{M}\left[\left(2a_1+(M-2)a_2\right)\bar{P}-\right. \\
& \left.\frac{1}{2}\left(4b_1+4b_2+2(M-4)b_3+2a_1^2+(M-2)a_2^2\right)\bar{P}^2\right]\log e+O(\bar{P}^3) \quad .
\end{aligned} \tag{B-16}$$

Finally, substituting $\{a_m\}$ and $\{b_m\}$ in (B-16), identifying $\dot{C}_{M\,\mathrm{ms}}^{IA}(0)$ and $\ddot{C}_{M\,\mathrm{ms}}^{IA}(0)$, and using the general expression of the low-SNR slope (B-5), (5-28) is obtained.

B.3 High-SNR Spectral Efficiency Slope

The high-SNR spectral efficiency slope of the optimum receiver is expressed in [6] as

$$S_\infty \triangleq \lim_{\bar{P}\to\infty}\bar{P}\dot{C}(\bar{P}) \quad , \tag{B-17}$$

where the derivative is with respect to the transmit SNR $\bar{P}$. Using (5-6) and (B-17), it follows that for $M\geq 2$

$$\begin{aligned}
S_{\infty\,\mathrm{opt}}^{IA} &= \lim_{\bar{P}\to\infty}\bar{P}\dot{C}_{M\,\mathrm{opt}}^{IA}(\bar{P}) \\
&= \lim_{\bar{P}\to\infty}\bar{P}\dot{\mathcal{C}}_M(\bar{P})-\frac{2}{M}\lim_{\bar{P}\to\infty}\bar{P}\dot{\mathcal{C}}_I(\bar{P}) \\
&= S_{\infty_{\mathrm{opt}}}^{M}-\frac{2}{M}S_{\infty_{\mathrm{opt}}}^{I} \quad ,
\end{aligned} \tag{B-18}$$

where $S^{M}_{\infty\,\mathrm{opt}}$ and $S^{I}_{\infty_{\mathrm{opt}}}$ are the high-SNR spectral efficiency slopes of the optimum receiver in the extended cluster setup, and in the isolated single cell setup, respectively. Using (3-14) and the definition of the extended cluster setup, it is easily verified that

$$S^{M}_{\infty\,\mathrm{opt}} = \min\left(\beta\left(1+\frac{2}{M}\right),1\right) \quad . \tag{B-19}$$

In addition, the high SNR slope in the single-cell setup is given by [6]

$$S^{I}_{\infty_{\mathrm{opt}}} = \min\left(\beta,1\right) \quad . \tag{B-20}$$

Finally, substituting (B-19) and (B-20) into (B-18), we get (5-26).

B.4 Spectral Efficiencies in the High Cell Load Region

B.4.1 Linear MMSE Receiver

In the high cell load region ($\beta \gg 1$), a finite transmit energy per bit implies that $\bar{P} \ll 1$, since from (3-9) $\beta\bar{P} = C\frac{E_b^t}{N_0}$ (with C being the spectral efficiency). In addition, examining the implicit equation for $\Gamma^{IA}(m)$ (5-16), it is concluded that a consistent solution to the equation exists, for $\beta \gg 1$, only if $\beta\Gamma^{IA}(m)$ is finite. Hence, $\beta\left(1+2\alpha^2\right)\Gamma^{IA}_{M}(m)$ is approximated well for $M \geq 2$ by

$$\begin{aligned}\beta\left(1+2\alpha^2\right)\Gamma^{IA}_{M}(m) &= \sum_{l=m-1}^{m+1}\frac{[\boldsymbol{\mathcal{P}}^{IA}_{M}]_{l,m}}{1+\sum_{k=l-1}^{l+1}[\boldsymbol{\mathcal{P}}^{IA}_{M}]_{l,k}\beta\bar{P}} + O(\beta^{-1}) \\ m &= 0,1,\ldots,M+1 \quad ,\end{aligned} \tag{B-21}$$

where out-of-range indices should be ignored. Using the special structure of the discrete-index asymptotic power profile for the infinite cell-array setup, as defined by (5-15), (B-21) boils down to

$$\begin{aligned}\beta\left(1+2\alpha^2\right)\Gamma^{IA}_{M}(m) &= \frac{a_m}{1+(1+2\alpha^2)\beta\bar{P}} + O(\beta^{-1}) \\ m &= 0,1,\ldots,M+1 \quad ,\end{aligned} \tag{B-22}$$

where

$$a_m = \begin{cases} \alpha^2 \ , & m = 0, M+1 \\ 1+\alpha^2 \ , & m = 1, M \\ 1+2\alpha^2 \ , & 2 \le m \le M-1 \end{cases} \quad . \tag{B-23}$$

Now, recalling that $\beta \gg 1$ implies $(1+2\alpha^2)\,\Gamma_M^{IA}(m)\beta\bar{P} \ll 1$, then every summand in the expression for the spectral efficiency of the linear MMSE receiver (5-23) can be expressed by

$$\beta \log\left(1+\Gamma_M^{IA}(m)(1+2\alpha^2)\beta\bar{P}\right) = \frac{a_m \beta\bar{P}}{1+(1+2\alpha^2)\beta\bar{P}} \log e + O(\beta^{-1}) \quad . \tag{B-24}$$

Finally, substituting (B-24) and (B-23) into (5-23), replacing $\beta\bar{P}$ by $\frac{E_b^t}{N_0} C_{M\,\mathrm{ms}}^{IA}$ and following some algebra, (5-31) is obtained.

B.4.2 Optimum Receiver

The spectral efficiency of the optimum receiver in the infinite cell-array setup is combined of two terms as given in (5-6). Starting with $\mathcal{C}_M$ as given by (5-20), it can be shown applying similar arguments to those used in Subsection B.4.1, that for $\beta \gg 1$ the first and third terms of (5-20) cancel each other (up to $O(\beta^{-1})$). Hence $\mathcal{C}_M$ can be approximated as

$$\mathcal{C}_M = \frac{1}{M}\sum_{m=1}^{M} \log\left(1+\sum_{k=m-1}^{m+1} \frac{[\boldsymbol{\mathcal{P}}_M^{IA}]_{m,k}\beta\bar{P}}{1+\Gamma_M^{IA}(k)(1+2\alpha^2)\beta\bar{P}}\right) + O(\beta^{-1}) \quad . \tag{B-25}$$

Recalling that $\beta\,(1+2\alpha^2)\,\Gamma^{IA}(m)\bar{P} \ll 1$ when $\beta \gg 1$, then (B-25) reduces to

$$\begin{aligned} \mathcal{C}_M &= \frac{1}{M}\sum_{m=1}^{M} \log\left(1+\sum_{k=m-1}^{m+1} [\boldsymbol{\mathcal{P}}_M^{IA}]_{m,k}\beta\bar{P}\right) + O(\beta^{-1}) \\ &= \log\left(1+\left(1+2\alpha^2\right)\beta\bar{P}\right) + O(\beta^{-1}) \quad , \end{aligned} \tag{B-26}$$

where the last equality is obtained by using the structure of the discrete-index asymptotic power profile of the infinite cell array setup, $\boldsymbol{\mathcal{P}}_M^{IA}$, as defined in (5-15).

The second term of (5-6) is the optimum receiver spectral efficiency of an isolated single cell setup where the received SNR is $\alpha^2\bar{P}$. Hence (see [5]), for $\beta \gg 1$ the spectral efficiency

of the optimum receiver in this setup is given by

$$\mathcal{C}_I = \log\left(1+\alpha^2\bar{P}\beta\right) + O(\beta^{-1}) \quad . \tag{B-27}$$

Finally, substituting (B-26) and (B-27) into (5-6), replacing $\beta\bar{P}$ with $\frac{E_b^t}{N_0}C_{M\,\mathrm{ms}}^{IA}$, and following some algebra, (5-30) is obtained.

C Low-SNR Slope with a Symbol-Level Interlevear

The channel transfer matrix in the circular cell-array setup $\boldsymbol{S}^{CS}$, as defined in (8-1), is a three-block diagonal matrix. Ignoring the interference factor α, each block is of the form of $\boldsymbol{SH}$ where $\boldsymbol{S}$ is an $N\times K$ signature matrix and $\boldsymbol{H}$ is a $K\times K$ diagonal channel fades matrix. Hence, the product matrix $\boldsymbol{S}^{CS\dagger}\boldsymbol{S}^{CS}$ is a five-block diagonal matrix. Examining (8-20), it observed that in order to evaluate the denominator of the equation, it is required to derive the power profile of the above product matrix. Considering the symmetrical structure of the setup, it is enough to focus on a single row of five $K\times K$ blocks. Furthermore, it is enough to consider the diagonal block (referred in the following to as $\boldsymbol{B}_0$), and the two off-diagonal blocks on its right (referred to in the following as $\boldsymbol{B}_1$ and $\boldsymbol{B}_2$).

Relating to an arbitrary block-row m $(1<m<M)$ of $\boldsymbol{S}^{CS}$, the diagonal block $\boldsymbol{B}_0$ of the product matrix $\boldsymbol{S}^{CS\dagger}\boldsymbol{S}^{CS}$ is given by

$$\boldsymbol{B}_0 = \alpha^2\boldsymbol{H}_{m-1,m}^{\dagger}\boldsymbol{S}_m^{\dagger}\boldsymbol{S}_m\boldsymbol{H}_{m-1,m}+\boldsymbol{H}_{m,m}^{\dagger}\boldsymbol{S}_m^{\dagger}\boldsymbol{S}_m\boldsymbol{H}_{m,m}+\alpha^2\boldsymbol{H}_{m+1,m}^{\dagger}\boldsymbol{S}_m^{\dagger}\boldsymbol{S}_m\boldsymbol{H}_{m+1,m} \quad . \tag{C-1}$$

Careful examination of the entries of the $K\times K$ matrix $\boldsymbol{B}_0$ reveals that in terms of power profile there are only two types of entries: diagonal entries and non-diagonal entries. Starting with the set of K diagonal entries, and focusing without loss of generality on $(\boldsymbol{B}_0)_{1,1}$, it is easily verified that

$$(\boldsymbol{B}_0)_{1,1} = \left(\alpha^2|(\boldsymbol{H}_{m-1,m})_{1,1}|^2+|(\boldsymbol{H}_{m,m})_{1,1}|^2+\alpha^2|(\boldsymbol{H}_{m+1,m})_{1,1}|^2\right)\sum_{i=1}^{N}|(\boldsymbol{S}_m)_{i,1}|^2 \quad . \tag{C-2}$$

With the assumption of binary random signatures, the second moment of a diagonal entry

is given by

$$E[|(\boldsymbol{B}_0)_{1,1}|^2] = m_4(1+2\alpha^4) + m_2^2(4\alpha^2+2\alpha^4) \quad , \tag{C-3}$$

where $m_2 = E[|a|^2]$ and $m_4 = E[|a|^4]$ are the second and forth power moments of an individual fading coefficient, respectively. Turning to the set $K^2 - K$ non-diagonal entries of $\boldsymbol{B_0}$, and focusing without loss of generality on $(\boldsymbol{B}_0)_{1,2}$, it is easily verified that

$$\begin{aligned}(\boldsymbol{B}_0)_{1,2} = \big(&\alpha^2(\boldsymbol{H}_{m-1,m})^*_{1,1}(\boldsymbol{H}_{m-1,m})_{2,2} + (\boldsymbol{H}_{m,m})^*_{1,1}(\boldsymbol{H}_{m,m})_{2,2} \\ &+ \alpha^2(\boldsymbol{H}_{m+1,m})^*_{1,1}(\boldsymbol{H}_{m+1,m})_{2,2}\big)\sum_{i=1}^{N}(\boldsymbol{S}_m)^*_{i,1}(\boldsymbol{S}_m)_{i,2} \quad ,\end{aligned} \tag{C-4}$$

and the respective second power moment of a non-diagonal entry is given by

$$E[|(\boldsymbol{B}_0)_{1,2}|^2] = \frac{m_2^2(1+2\alpha^4)}{N} \quad . \tag{C-5}$$

The off-diagonal block $\boldsymbol{B}_1$ is given by

$$\boldsymbol{B}_1 = \alpha\boldsymbol{H}^{\dagger}_{m,m}\boldsymbol{S}^{\dagger}_m\boldsymbol{S}_{m+1}\boldsymbol{H}_{m,m+1} + \alpha\boldsymbol{H}^{\dagger}_{m+1,m}\boldsymbol{S}^{\dagger}_m\boldsymbol{S}_{m+1}\boldsymbol{H}_{m+1,m+1} \quad . \tag{C-6}$$

Examining the entries of $\boldsymbol{B}_1$ it is concluded that in terms of power profile all K^2 entries of the matrix are of the same type. Hence, it is enough to inspect $(\boldsymbol{B}_1)_{1,1}$ which is given by

$$(\boldsymbol{B}_1)_{1,1} = \alpha\left((\boldsymbol{H}_{m,m})^*_{1,1}(\boldsymbol{H}_{m,m+1})_{1,1} + (\boldsymbol{H}_{m+1,m})^*_{1,1}(\boldsymbol{H}_{m+1,m+1})_{1,1}\right)\sum_{i=1}^{N}(\boldsymbol{S}_m)^*_{i,1}(\boldsymbol{S}_{m+1})_{i,1} \quad , \tag{C-7}$$

and its respective second power moment equals to

$$E[|(\boldsymbol{B}_1)_{1,1}|^2] = \frac{2\alpha^2 m_2^2}{N} \quad . \tag{C-8}$$

The second off-diagonal block $\boldsymbol{B}_2$ is given by

$$\boldsymbol{B}_2 = \alpha^2\boldsymbol{H}^{\dagger}_{m+1,m}\boldsymbol{S}^{\dagger}_m\boldsymbol{S}_{m+2}\boldsymbol{H}_{m+1,m+2} \quad . \tag{C-9}$$

Examining the entries of $\boldsymbol{B}_2$ it is concluded that, as observed for $\boldsymbol{B}_1$, all K^2 entries of the

matrix have the same second power moment. Hence, it is enough to inspect $(\boldsymbol{B}_2)_{1,1}$ which is given by

$$(\boldsymbol{B}_2)_{1,1} = \alpha^2 (\boldsymbol{H}_{m+1,m})^*_{1,1} (\boldsymbol{H}_{m+1,m+2})_{1,1} \sum_{i=1}^{N} (\boldsymbol{S}_m)^*_{i,1} (\boldsymbol{S}_{m+2})_{i,1} \quad , \tag{C-10}$$

and its respective second power moment equals

$$E[|(\boldsymbol{B}_2)_{1,1}|^2] = \frac{\alpha^4 m_2^2}{N} \quad . \tag{C-11}$$

Now, combining (C-3), (C-8) and (C-11), the denominator of (8-20) can be expressed as

$$\begin{aligned} & E\left[\text{trace}\left\{\left(\boldsymbol{S}^{CS\dagger}\boldsymbol{S}^{CS}\right)^2\right\}\right] = \sum_{i=1}^{MK}\sum_{j=1}^{MK} E\left[|(\boldsymbol{S}^{CS\dagger}\boldsymbol{S}^{CS})_{i,j}|^2\right] \\ & = M\left(KE[|(\boldsymbol{B}_0)_{1,1}|^2] + (K^2-K)E[|(\boldsymbol{B}_0)_{1,2}|^2] + 2K^2E[|(\boldsymbol{B}_1)_{1,1}|^2] + 2K^2E[|(\boldsymbol{B}_2)_{1,1}|^2]\right) \\ & = MK\left(\left[m_4 + \left(\frac{K}{N} - \frac{1}{N}\right)m_2^2\right] + 4m_2^2\left[1+\frac{K}{N}\right]\alpha^2 + 2\left[m_4 + \left(1+2\frac{K}{N} - \frac{1}{N}\right)m_2^2\right]\alpha^4\right). \end{aligned} \tag{C-12}$$

The nominator of (8-20) equals

$$\begin{aligned} \left(E\left[\text{trace}\left\{\boldsymbol{S}^{CS\dagger}\boldsymbol{S}^{CS}\right\}\right]\right)^2 &= \left(\sum_{i=1}^{MN}\sum_{j=1}^{MK} E\left[|(\boldsymbol{S}^{CS})_{i,j}|^2\right]\right)^2 \\ &= M^2K^2m_2^2(1+2\alpha^2)^2 \quad . \end{aligned} \tag{C-13}$$

Combining (C-13) and (C-12) the low-SNR spectral efficiency slope of the optimum receiver is given by

$$S_0^{CS}{}_{\text{opt}} = \frac{2\frac{K}{N}(1+2\alpha^2)^2}{\left[\mathcal{K} + \frac{K}{N} - \frac{1}{N}\right] + 4\left[1+\frac{K}{N}\right]\alpha^2 + 2\left[\mathcal{K}+1+2\frac{K}{N}-\frac{1}{N}\right]\alpha^4} \quad . \tag{C-14}$$

Finally, recalling the asymptotic nature of the model in concern where $N, K \to \infty$ while $\frac{K}{N} \to \beta$, (C-14) can be rewritten as

$$S_0^{CS}{}_{\text{opt}} = \frac{2\beta(1+2\alpha^2)^2}{[\mathcal{K}+\beta] + 4[1+\beta]\alpha^2 + 2[\mathcal{K}+1+2\beta]\alpha^4} \quad . \tag{C-15}$$

Additional minor algebra is needed to express (C-15) as (8-21) and (8-22).

D Low-SNR Spectral Efficiency Slope - No Fading

The derivation in this appendix follows closely the argumentation and procedures employed in App. C, while accounting for the absence of fading. Accordingly, the diagonal block $\boldsymbol{B}_0$ of the product matrix $\boldsymbol{S}^{CNF\dagger}\boldsymbol{S}^{CNF}$ equals

$$\boldsymbol{B}_0 = \left(1+2\alpha^2\right)\boldsymbol{S}_m^{\dagger}\boldsymbol{S}_m \quad . \tag{D-1}$$

Careful examination of the entries of the $K \times K$ matrix $\boldsymbol{B}_0$ reveals that, as was the case for the symbol-interleaved setup, in terms of power profile there are only two types of entries: diagonal entries and non-diagonal entries. Starting with the K diagonal entries, and focusing without loss of generality on $(\boldsymbol{B}_0)_{1,1}$, it is verified that

$$(\boldsymbol{B}_0)_{1,1} = \left(1+2\alpha^2\right)\sum_{i=1}^{N}|(\boldsymbol{S}_m)_{i,1}|^2 \quad . \tag{D-2}$$

With the assumption of binary random signatures, the second power moment of a diagonal entry is given by

$$E[|(\boldsymbol{B}_0)_{1,1}|^2] = (1+2\alpha^2)^2 \quad . \tag{D-3}$$

Turning to the set of K^2-K non-diagonal entries, and considering without loss of generality $(\boldsymbol{B}_0)_{1,2}$, it is easily verified that

$$(\boldsymbol{B}_0)_{1,2} = \left(1+2\alpha^2\right)\sum_{i=1}^{N}(\boldsymbol{S}_m)_{i,1}^{*}(\boldsymbol{S}_m)_{i,2} \quad , \tag{D-4}$$

and the respective second power moment of a non-diagonal entry is given by

$$E[|(\boldsymbol{B}_0)_{1,2}|^2] = \frac{(1+2\alpha^2)^2}{N} \quad . \tag{D-5}$$

The off-diagonal block $\boldsymbol{B}_1$ is given by

$$\boldsymbol{B}_1 = \alpha \boldsymbol{S}_m^{\dagger} \boldsymbol{S}_{m+1} \quad . \tag{D-6}$$

Examining the entries of $\boldsymbol{B}_1$ it is concluded that all K^2 entries have the same power profile. Hence, it is enough to consider $(\boldsymbol{B}_1)_{1,1}$ which is given by

$$(\boldsymbol{B}_1)_{1,1} = 2\alpha \sum_{i=1}^{N} (\boldsymbol{S}_m)_{i,1}^{*} (\boldsymbol{S}_{m+1})_{i,1} \quad , \tag{D-7}$$

and its respective second power moment equals

$$E[|(\boldsymbol{B}_1)_{1,1}|^2] = \frac{4\alpha^2}{N} \quad . \tag{D-8}$$

The second off-diagonal block $\boldsymbol{B}_2$ is given by

$$\boldsymbol{B}_2 = \alpha^2 \boldsymbol{S}_m^{\dagger} \boldsymbol{S}_{m+2} \quad . \tag{D-9}$$

Examining the entries of $\boldsymbol{B}_2$ it is concluded that all K^2 entries have the same second power moment. Hence, it is enough to inspect $(\boldsymbol{B}_2)_{1,1}$ which is given by

$$(\boldsymbol{B}_2)_{1,1} = \alpha^2 \sum_{i=1}^{N} (\boldsymbol{S}_m)_{i,1}^{*} (\boldsymbol{S}_{m+2})_{i,1} \quad , \tag{D-10}$$

and its second power moment equals

$$E[|(\boldsymbol{B}_2)_{1,1}|^2] = \frac{\alpha^4}{N} \quad . \tag{D-11}$$

Combining (D-3), (D-8) and (D-11), the denominator of (8-20) can be expressed as

$$\begin{aligned} E\left[\text{trace}\left\{\left(\boldsymbol{S}^{CNF\dagger}\boldsymbol{S}^{CNF}\right)^2\right\}\right] &= \sum_{i=1}^{MK}\sum_{j=1}^{MK} E\left[|(\boldsymbol{S}^{CNF\dagger}\boldsymbol{S}^{CNF})_{i,j}|^2\right] \\ &= M\left(KE[|(\boldsymbol{B}_0)_{1,1}|^2] + (K^2-K)E[|(\boldsymbol{B}_0)_{1,2}|^2] + 2K^2E[|(\boldsymbol{B}_1)_{1,1}|^2] + 2K^2E[|(\boldsymbol{B}_2)_{1,1}|^2]\right) \\ &= MK\left(\left[1+\frac{K}{N}-\frac{1}{N}\right] + 4\left[1+3\frac{K}{N}-\frac{1}{N}\right]\alpha^2 + 2\left[2+3\frac{K}{N}-\frac{2}{N}\right]\alpha^4\right). \end{aligned} \tag{D-12}$$

The nominator of (8-20) equals to

$$\begin{aligned} \left(E\left[\text{trace}\left\{\boldsymbol{S}^{CNF\dagger}\boldsymbol{S}^{CNF}\right\}\right]\right)^2 &= \left(\sum_{i=1}^{MN}\sum_{j=1}^{MK} E\left[|(\boldsymbol{S}^{CNF})_{i,j}|^2\right]\right)^2 \\ &= M^2K^2(1+2\alpha^2)^2 \quad . \end{aligned} \tag{D-13}$$

Using (D-13) and (D-12) the low-SNR spectral efficiency slope of the optimum receiver is given by

$$S_0^{CNF}{}_{\text{opt}} = \frac{2\frac{K}{N}(1+2\alpha^2)^2}{\left[1+\frac{K}{N}-\frac{1}{N}\right] + 4\left[1+3\frac{K}{N}-\frac{1}{N}\right]\alpha^2 + 2\left[2+3\frac{K}{N}-\frac{2}{N}\right]\alpha^4} \quad . \tag{D-14}$$

Finally, applying the asymptotic nature the system model in concern it follows that

$$S_0^{CNF}{}_{\text{opt}} = \frac{2\beta(1+2\alpha^2)^2}{[1+\beta] + 4[1+3\beta]\alpha^2 + 2[2+3\beta]\alpha^4} \quad , \tag{D-15}$$

and with some minor algebra (D-15) can be expressed as (8-24).

References

[1] S. Verdú, *Multiuser Detection*. Cambridge, UK: Cambridge University Press, 1998.

[2] J. W. Silverstein and Z. D. Bai, "On the empirical distribution of eigenvalues of a class of large dimensional random matrices," *Journal of Multivariate Analysis*, vol. 54, pp. 175–192, 1995.

[3] J. W. Silverstein, "Strong convergence of the empirical distribution of eigenvalues of large dimensional random matrices," *Journal of Multivariate Analysis*, vol. 55, pp. 331–339, 1995.

[4] V. L. Girko, *Theory of Random Determinants*. Kluwer, 1990.

[5] S. Verdú and S. Shamai (Shitz), "Spectral efficiency of CDMA with random spreading," *IEEE Transactions on Information Theory*, vol. 45, pp. 622–640, Mar. 1999.

[6] S. Shamai (Shitz) and S. Verdú, "The impact of frequency-flat fading on the spectral efficiency of CDMA," *IEEE Transactions on Information Theory*, vol. 47, pp. 1302–1327, May 2001.

[7] D. Guo, S. Shamai (Shitz), and S. Verdú, "Mutual information and MMSE in Gaussian channels," in *Proceedings of the International Symposium on Information Theory (ISIT2004)*, June 27 – July 2, 2004.

[8] D. Tse and S. Hanly, "Linear multiuser receivers: Effective interference, effective bandwidth and user capacity," *IEEE Transactions on Information Theory*, vol. 45, pp. 641–657, Mar. 1999.

[9] Kiran and D. N. C. Tse, "Effective interference and effective bandwidth of linear multiuser receivers in asynchronous systems," *IEEE Transactions on Information Theory*, vol. 46, no. 4, pp. 1426–1447, 2000.

[10] S. V. Hanly and D. N. C. Tse, "Resource pooling and effective bandwidths in CDMA networks with multiuser receivers and spatial diversity," *IEEE Transactions on Information Theory*, vol. 47, pp. 1328–1351, May 2001.

[11] A. D. Wyner, "Shannon-theoretic approach to a Gaussian cellular multiple-access channel," *IEEE Transactions on Information Theory*, vol. 40, pp. 1713–1727, Nov. 1994.

[12] S. Shamai (Shitz) and A. D. Wyner, "Information-theoretic considerations for symmetric, cellular, multiple-access fading channels - Parts I & II," *IEEE Transactions on Information Theory*, vol. 43, pp. 1877–1911, Nov. 1997.

[13] O. Somekh and S. Shamai (Shitz), "Shannon-theoretic approach to Gaussian cellular multi-access channel with fading," *IEEE Transactions on Information Theory*, vol. 46, pp. 1401–1425, July 2000.

[14] B. M. Zaidel, S. Shamai (Shitz), and S. Verdú, "Multi-cell uplink spectral efficiency of coded DS-CDMA with random signatures," *IEEE Journal on Selected Areas in Communications*, vol. 19, pp. 1556–1569, Aug. 2001. See also: — "Spectral Efficiency of Randomly Spread DS-CDMA in a Multi-Cell Model," Proceedings of the 37th Annual Allerton Conference on Communication, Control and Computing, Monticello, IL, pp. 841–850, Sept. 1999.

[15] B. M. Zaidel, S. Shamai (Shitz), and S. Verdú, "Multi-cell uplink spectral efficiency of randomly spread DS-CDMA in Rayleigh fading channels," in *Proceedings of the 6th International Symposium on Communication Techniques and Applications (ISCTA'01)*, (Ambleside, UK), pp. 499–504, July 15 – 20, 2001. See also: —, "Random CDMA in the multiple cell uplink environment: the effect of fading on various receivers," Proceedings of the 2001 IEEE Information Theory Workshop, Cairns, Australia, Sept. 2–7, 2001, pp. 42–45.

[16] A. M. Tulino, S. Verdú, and A. Lozano, "Capacity of antenna arrays with space polarization and pattern diversity," in *Proceedings of 2003 IEEE Information Theory Workshop (ITW2003)*, (Paris, France), pp. 324–327, Mar. 31 – Apr. 4, 2003.

[17] S. Verdú, "Spectral efficiency in the wideband regime," *IEEE Transactions on Information Theory*, vol. 48, pp. 1329–1343, June 2002.

[18] F. D. Neeser and J. L. Massey, "Proper complex random processes with applications to information theory," *IEEE Transactions on Information Theory*, vol. 39, pp. 1293–1302, July 1993.

[19] A. M. Tulino and S. Verdú, "Random matrix theory and wireless communications," *Foundations and Trends in Communications and Information Theory*, 2004. To Appear.